

Auxiliary-Fermion Approach to Critical Fluctuations in the 2D Quantum AF Heisenberg Model

Jan Brinckmann and Peter Wölfle

Institut für Theorie der Kondensierten Materie, Universität Karlsruhe, D-76128 Karlsruhe, Germany

(Dated: 19.05.04)

The nearest-neighbor quantum-antiferromagnetic (AF) Heisenberg model for spin 1/2 on a two-dimensional square lattice is studied in the auxiliary-fermion representation. Expressing spin operators by canonical fermionic particles requires a constraint on the fermion charge $Q_i = 1$ on each lattice site i , which is imposed approximately through the thermal average. The resulting interacting fermion system is first treated in mean-field theory (MFT), which yields an AF ordered ground state and spin waves in quantitative agreement with conventional spin-wave theory. At finite temperature a self-consistent approximation beyond mean field is required in order to fulfill the Mermin–Wagner theorem. We first discuss a fully self-consistent approximation, where fermions are renormalized due to fluctuations of their spin density, in close analogy to FLEX. While static properties like the correlation length, $\xi(T) \propto \exp(a J/T)$, come out correctly, the dynamical response lacks the magnon-like peaks which would reflect the appearance of short-range order at low T . This drawback, which is caused by overdamping, is overcome in a ‘minimal self-consistent approximation’ (MSCA), which we derive from the equations of motion. The MSCA features dynamical scaling at small energy and temperature and is qualitatively correct both in the regime of order-parameter relaxation at long wavelengths $\lambda > \xi$ and in the short-range-order regime at $\lambda < \xi$. We also discuss the impact of vertex corrections and the problem of pseudo-gap formation in the single-particle density of states due to long-range fluctuations. Finally we show that the (short-range) magnetic order in MFT and MSCA helps to fulfill the constraint on the local fermion occupancy.

PACS numbers:

I. INTRODUCTION

Antiferromagnetic correlations play an important role in the physics of high-temperature superconductors. Magnetism is most pronounced in the undoped parent compounds, where the almost uncoupled two-dimensional CuO-planes form magnetic Mott insulators with one spin-1/2 electron per Cu-site. The simplest model for a CuO-plane is the quantum Heisenberg antiferromagnet (QHAF) in two dimensions (2D) on a square lattice,

$$H = \frac{1}{2} \sum_{i,j} J_{ij} \mathbf{S}_i \mathbf{S}_j \quad (1)$$

The super-exchange coupling $J_{ij} = J > 0$ is non-zero only if the Cu-sites i, j are nearest neighbors. In the undoped compounds studied experimentally, it assumes values around $J \simeq 130$ meV.

This model has been studied intensively in the past¹. Its ground state at zero temperature $T = 0$ appears to be a Néel state with an order parameter $|\langle \mathbf{S} \rangle|$ moderately reduced from its classical value 1/2 by quantum fluctuations. At finite temperature $T > 0$ the theorem of Mermin and Wagner prohibits any long-range order. For sufficiently low T the magnetic correlation length ξ grows exponentially in the two-dimensional system and diverges at $T = 0$,

$$\xi(T) \propto \exp(a J/T) \quad (2)$$

ξ is measured in units of the lattice spacing, which is set to 1. In the following we also use $\hbar \equiv 1$, $k_B \equiv$

1. The exponential factor in $\xi(T)$ has been obtained from quantum-monte-carlo (QMC) calculation^{2,3,4} of the QHAF, high-temperature series expansion⁵, Schwinger-boson mean-field theory⁶ (SBMFT), and modified spin-wave theory⁷. The exponent comes out^{2,3,6} as $a \simeq 1.15$. An exponential behavior like Eq.(2) also results from the (classical) non-linear sigma model^{8,9} (NL σ M) as well as the quantum NL σ M (QNL σ M) in the so-called renormalized classical regime^{10,11,12}.

The theoretical predictions from the QHAF and the (Q)NL σ M are consistent with experiments on undoped cuprates above their respective Néel temperature T_N , confirming the almost two-dimensional nature of fluctuations in these systems. In particular, a correlation length behaving like Eq.(2) has been seen in quasi-elastic (energy integrated) neutron scattering on $\text{Sr}_2\text{Cu}_3\text{O}_4\text{Cl}_2$ (Ref. 13), $\text{Sr}_2\text{CuO}_2\text{Cl}_2$ (Ref. 14), and La_2CuO_4 (Ref. 15,16,17). The observed^{13,14,15} exponent $a = 1.15$ agrees with theory. A three-dimensional (algebraic) behavior might be observable^{13,14} at temperatures very close to T_N .

The dynamics of spin fluctuations are measured through the dynamical structure factor $S(\mathbf{q}, \omega)$. In general two regimes are expected, depending on the wave vector $\mathbf{k} = \mathbf{q} - \mathbf{Q}$ relative to the Néel ordering vector $\mathbf{Q} = (\pi, \pi)$: For $k\xi \ll 1$, i.e., for distances much longer than the correlation length, the spectrum S shows a single peak at $\omega = 0$ with some width $\sim \omega_0$ that depends weakly on $k\xi$. The energy scale ω_0 represents the time scale for relaxation of the order parameter in the disordered phase $T > 0$. Critical slowing down leads to a vanishing of ω_0 like $\omega_0 \sim \xi^{-z}$ as $T \rightarrow 0$. The dynamical

exponent z comes out as $z = 1$. For $k\xi \gg 1$ the peak position shifts to finite ω and becomes k -dependent, reminiscent of damped spin waves. These originate from the short-range magnetic order, which is visible at distances short compared to the correlation length. Moreover, the dynamical scaling hypothesis¹¹ states that for $\xi \gg 1$ and all $k \ll \pi$ spin fluctuations are governed by the single energy scale ω_0 ; the structure factor obeys the scaling form

$$S(\mathbf{q}, \omega) = \frac{1}{\omega_0} S^{st}(\mathbf{q}) \Phi(k\xi, \omega/\omega_0) \quad (3)$$

with the static structure factor (equal-time correlation function)

$$S^{st}(\mathbf{q}) = \langle S_{\mathbf{q}}^x S_{-\mathbf{q}}^x \rangle = S^{st}(\mathbf{Q}) \varphi(k\xi). \quad (4)$$

φ and Φ denote (a priori unknown) scaling functions. The dynamical structure factor has been calculated¹⁸ using the QMC plus maximum-entropy method for the QHAF, molecular dynamics (MD) on the classical Heisenberg model¹⁹, the SBMFT^{20,21}, and MD on a classical lattice model²² equivalent to the QNL σ M in the renormalized classical regime¹¹. The form (3) of the structure factor, the presence of propagating modes in the ‘shape function’ Φ for $k\xi > 1$, and the energy scale $\omega_0 \sim \xi^{-1}$ have been well confirmed. The latter has also been calculated from coupled-mode theory²³. Experimentally, inelastic neutron scattering (INS) on several cuprate parent compounds^{24,25,26} at temperatures $T > T_N$ shows a quasi-elastic peak at zero energy, the observed²⁴ dynamical exponent is $z = 1$. The latter is also found in magnetic resonance²⁷. The INS data is consistent to spin-wave like excitations at higher energies²⁵ in the paramagnetic phase.

Results for the dynamics of spin fluctuations come primarily from purely numerical approaches like QMC and MD. For an analytical treatment of the Heisenberg model, the non-canonical commutation relations of spin operators S^x, S^y, S^z pose a severe difficulty. This can be circumvented by re-writing S^μ in canonical boson or fermion creation and annihilation operators. These act on an enlarged Hilbert space that contains unphysical states, which have to be removed by imposing a constraint. Using Schwinger bosons b_n , $n = 1, 2$, the spin-1/2 operator and constraint read⁶

$$\mathbf{S} = \frac{1}{2} \sum_{n,n'=1,2} b_n^\dagger \boldsymbol{\sigma}^{nn'} b_{n'} \quad , \quad \sum_{n=1,2} b_n^\dagger b_n = 1$$

Alternatively, one can use Abrikosov auxiliary fermions^{28,29} f_\uparrow, f_\downarrow that carry spin-1/2,

$$\mathbf{S}_i = \frac{1}{2} \sum_{\alpha, \alpha'=\pm 1} f_{i\alpha}^\dagger \boldsymbol{\sigma}^{\alpha\alpha'} f_{i\alpha'} \quad , \quad Q_i = \sum_\alpha f_{i\alpha}^\dagger f_{i\alpha} = 1 \quad (5)$$

Here a lattice-site index i has been added; $\alpha = +1, -1$ corresponds to \uparrow, \downarrow .

The fermion representation (5) of the Heisenberg model (1) is actually the 1/2-filled (undoped) limit of the standard slave-boson formulation of the t - J -model. The latter has been extensively studied using, e.g., mean-field theory³⁰. These works focus on the superconducting and normal-state properties of the t - J -model at finite hole filling (doping), and its application to the doped cuprate superconductors³⁰. At low hole concentration and in particular at 1/2-filling the slave-boson mean-field theory gives antiferromagnetic (AF) long-range order^{31,32}. The strong magnetic correlations at finite temperature in the 2D system, however, have not been considered in this type of approach.

The purpose of this paper is to study the antiferromagnetic spin-1/2 Heisenberg model (QHAF) on a strictly two dimensional square lattice at finite temperature, using the auxiliary-fermion representation (5). In contrast to the boson approach^{6,20}, mean-field theory with fermions is merely useful for the AF ordered ground state. In mean-field approximation the fermions form a spin-density-wave state below a finite Néel temperature $T_N = 0.5 J$. Thus, at $T > 0$ a self-consistent T-matrix approximation beyond mean-field is required in order to suppress the phase transition. Two approximation schemes will be proposed and compared to the established results reviewed above. A suitable approximation should be able to fulfill the Mermin–Wagner theorem and reproduce the exponentially growing magnetic correlation length, also it should yield a qualitatively correct description of the dynamics including critical slowing down and short-range order. Once the important elements of such an approximation are identified, the theory can possibly be extended to less well understood cases, e.g., the t - J -model at finite hole filling by introducing ‘slave’ bosons for the doped holes.

The present study is related to certain self-consistent diagrammatic schemes for the 2D Hubbard model, like the FLEX approximation³³: When the magnetic correlation length is growing (e.g., due to a reduction of hole filling) the density of states of electrons is expected to develop a pseudo precursor gap³⁴ around the Fermi level, reflecting the proximity to an AF ordered state which is characterized by zero spectral weight at the Fermi energy. It has been demonstrated³⁵ that an approximation with ‘reduced self-consistency’, i.e., where part of the electron lines in the self energy are replaced by bare ones, favor the formation of such a spectral-weight suppression. A similar observation is made here: our approximation with reduced self-consistency (presented in Sect. V) is able to produce a propagating spin-wave-like mode reflecting short-range order, and the spectrum of auxiliary fermions shows a pseudo gap. In the fully self-consistent approximation (built in close analogy to FLEX), on the other hand, ‘spin-wave’ mode and pseudo gap are absent. The related problem of strong collective Cooper-pair fluctuations in the normal state of 2D superconductors has been studied in the past^{36,37,38}. The connection of these approaches to the present work is considered in Sect. V

and Appendix D.

The order of the paper is as follows: The auxiliary-fermion formulation is introduced in detail in the next Section II, and the mean-field theory is discussed in the following Sect. III. At zero temperature the mean-field theory resembles linear spin-wave theory³⁹ (SWT), but is useless at $T > 0$. In Sect. IV the fully self-consistent diagrammatic approximation is presented. Static and dynamical properties are calculated by analytical and numerical solution of the self-consistent integral equations. In Sect. V the above-mentioned approximation with reduced self-consistency is explored in detail. It leads to results that qualitatively agree very well with what is known about the QHAF and the QNL σ M at low temperature. In Sect. IV C we apply the conserving-approximation method and demonstrate its impact on the results obtained in Sect. IV, and finally in Sect. VI we estimate the fluctuations of the fermion charge Q_i . The paper closes with a conclusion and some technical appendices. Calculations are performed at low temperatures $T < 0.2 J$, where scaling is observed. A possible crossover to quantum-critical behavior^{3,10,40} at higher temperatures is not considered.

II. AUXILIARY-FERMION FORMULATION

The constraint in Eq.(5) requires the fermion charge to be fixed to 1 at each lattice site i individually. This projection can be performed exactly in models like the Anderson impurity and Kondo model^{41,42,43}, which possess just one atomic orbital with strong electron-electron interaction. In models containing a whole lattice of such orbitals the exact projection leads to a loss of the linked-cluster theorem, which prohibits infinite-order resummation of the perturbation series^{44,45} and self-consistent approximations based on the skeleton-diagram expansion. The limit of infinite spatial dimension^{46,47} has frequently been used to circumvent this problem. An alternative is to start from a mean-field theory⁴⁸, where the constraint is observed only in the thermal average. For the present case this reads,

$$Q_i \rightarrow \langle Q_i \rangle = \langle Q_1 \rangle = \sum_{\alpha} \langle f_{1\alpha}^{\dagger} f_{1\alpha} \rangle = 1 \quad (6)$$

and is introduced into the Hamiltonian (1), (5) through a chemical potential μ^f for the fermions. Due to particle-hole symmetry⁴⁹ it is $\mu^f = 0$. The partition function can now be written as a standard coherent-state path integral⁵⁰,

$$Z[h] = \int \mathcal{D}[f, \bar{f}] e^{-A} \quad (7)$$

with the action $A = A^0 + A^h + A^J$,

$$A^0 = \int_0^{\beta} d\tau \sum_{i,\alpha} \bar{f}_{i\alpha}(\tau) [\partial_{\tau} - \mu^f] f_{i\alpha}(\tau) \quad (8a)$$

$$A^h = - \int_0^{\beta} d\tau \sum_i \mathbf{h}_i(\tau) \mathbf{S}_i(\tau) \quad (8b)$$

$$A^J = \int_0^{\beta} d\tau \frac{1}{2} \sum_{i,j} J_{ij} \mathbf{S}_i(\tau) \mathbf{S}_j(\tau) \quad (8c)$$

with anticommuting Grassmann variables f, \bar{f} , and $\beta = 1/k_B T \equiv 1/T$. An arbitrary magnetic source field \mathbf{h} has been added. The underlying lattice is a d -dimensional cubic lattice with lattice spacing $a \equiv 1$; only the two-dimensional (2D) case $d = 2$ will be studied in detail.

In the following the connected spin propagator is considered,

$$\begin{aligned} \chi_{ij}^{\mu\mu'}(\tau, \tau') &= \langle \mathcal{T}_{\tau} S_i^{\mu}(\tau) S_j^{\mu'}(\tau') \rangle_{conn} \quad (9) \\ &= \langle \mathcal{T}_{\tau} S_i^{\mu}(\tau) S_j^{\mu'}(\tau') \rangle - \langle S_i^{\mu}(\tau) \rangle \langle S_j^{\mu'}(\tau') \rangle \end{aligned}$$

where $\mu = x, y, z$ denotes the spin component. It is calculated using a Feynman-diagram expansion⁵⁰ with A^J as perturbation. This will involve the Green's function of fermions,

$$\begin{aligned} [\bar{G}_{ij}(\tau, \tau')]^{\alpha\alpha'} &= -\langle \mathcal{T}_{\tau} f_{i\alpha}(\tau) f_{j\alpha'}^{\dagger}(\tau') \rangle \quad (10) \\ &= -\langle f_{i\alpha}(\tau) \bar{f}_{j\alpha'}(\tau') \rangle \end{aligned}$$

Time- τ ordered expectation values are calculated via

$$\langle M \rangle = \frac{1}{Z[h]} \int \mathcal{D}[f, \bar{f}] e^{-A} M \quad (11)$$

Note that the fermion Green's function \bar{G} is not an observable quantity, since it depends on local $U(1)$ gauge transformations⁵¹ of $f_{i\alpha}, f_{i\alpha}^{\dagger}$. The susceptibility χ , on the contrary, is built from the gauge-invariant physical observables Eq.(5).

It is of great help that we can make use of standard Feynman-diagram techniques for a perturbation expansion in the interaction A^J . This requires a mean-field like treatment of the constraint Eq.(6), since then perturbation theory starts from (effectively) free fermions and Wick's theorem can be applied. In principle the treatment of the constraint can be improved by generalizing the chemical potential μ^f to a fluctuating Lagrange multiplier⁴³, but we restrict ourselves to the simplest approach⁵². Nevertheless, in the self-consistent approximations to be discussed below the pseudo fermions do not develop a finite hopping amplitude connecting different lattice sites i, j ,

$$\langle f_{i\alpha}^{\dagger} f_{j\alpha'} \rangle \propto \delta_{ij}$$

and anomalous expectation values of the form

$$\langle f_{i\alpha} f_{j\alpha'} \rangle = 0$$

are absent. As a consequence the Green's function of fermions is always local, i.e.,

$$\bar{G}_{ij} = \delta_{ij} \bar{G}_i \quad (12)$$

That is, the auxiliary fermions cannot develop any dispersion. Since unphysical expectation values are zero the local charge Q_i introduced in Eq.(6) is most likely conserved. Therefore spurious unphysical contributions to physical correlators like Eq.(9) are due to states with $Q_i \neq 1$ introduced by the trace in the thermal average Eq.(11), but these are not generated dynamically. We return to this issue later in Sect. VI.

III. MEAN-FIELD THEORY USING AUXILIARY FERMIONS

The Heisenberg term A^J is a two-particle interaction. A mean-field decomposition of A^J leads to an effective Hamiltonian^{31,32,53,54} with self-consistent order parameters $\sum_{\alpha,\alpha'} \langle f_{i\alpha}^\dagger \sigma^{\alpha\alpha'} f_{i\alpha'} \rangle = 2\langle \mathbf{S}_i \rangle$, $\langle f_{i\alpha}^\dagger f_{j\alpha} \rangle$, $\langle f_{i\uparrow}^\dagger f_{j\downarrow} \rangle$. These correspond to phases with different spontaneously broken symmetries, namely magnetic order, the so-called resonating valence bond⁵⁵ (RVB) or the flux phase^{29,56}, and a d-wave paired state of the fermions^{57,58,59}, respectively. In the undoped case considered here, the latter two are equivalent by particle-hole symmetry⁴⁹. The flux and the paired state order parameters are unphysical, but may correspond to physical regimes observed experimentally (the pseudo-gap regime in the cuprates). The respective transition temperatures are interpreted as crossovers. The magnetic order parameter $\sum_{\alpha,\alpha'} \langle f_{i\alpha}^\dagger \sigma^{\alpha\alpha'} f_{i\alpha'} \rangle$, on the other hand, is a physical (gauge invariant) quantity; a non-zero value indicates a true phase transition. If the free energies of these phases are compared in an unrestricted mean-field calculation, it turns out^{31,32} that only $\langle \mathbf{S} \rangle$ becomes finite in the Heisenberg model, indicating a Néel-ordered phase below some transition temperature $T_N \sim J$. This is consistent with the fact that the ground state of the Heisenberg model is close to Néel order¹. Only for finite hole filling in the t - J -model a phase is observed at low T , where AF and d-wave pairing order coexist³². Therefore we do not consider flux or pairing instabilities in the following.

Note that the large- N approach^{29,56} leads to a different ground state: The spin-index of the fermions is generalized from 2 to N states, and the limit $N \rightarrow \infty$ leads to a saddle-point theory giving a flux phase with $\langle f_{i\alpha}^\dagger f_{j\alpha} \rangle \neq 0$, while magnetism is suppressed.

A. AF Order and Spin Waves

With the source-field \mathbf{h} set to zero, the Green's function (10), (12) of the fermions reads

$$\bar{G}_i(i\omega) = [i\omega + \mu^f - \bar{\Sigma}_i(i\omega)]^{-1} \quad (13)$$

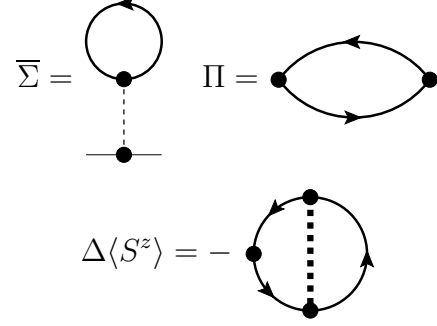


FIG. 1: Diagrammatic representation of $\bar{\Sigma}$, Π , $\Delta\langle S^z \rangle$ in mean-field approximation, Sect. III A. The thin dashed line is the bare interaction J in Eq.(8c), the thick dashed line the renormalized one Eq.(30), and the full lines are the Green's function of pseudo fermions Eq.(13) in mean-field approximation, Eq.(15). The dots represent Pauli matrices $\times 1/2$. A closed fermion loop requires a trace in spin space.

$\omega = (2n+1)\pi/\beta$ denotes a fermionic Matsubara frequency, \bar{G} and $\bar{\Sigma}$ are matrices in spin space, and the chemical potential is always $\mu^f = 0$ by particle-hole symmetry. In mean-field the self energy $\bar{\Sigma}_i$ is given by the self-consistent Hartree approximation depicted in Fig. 1 and reads

$$\begin{aligned} \bar{\Sigma}_i(i\omega) &= \sum_j J_{ij} \frac{1}{2} \sigma \frac{1}{2} \text{Tr}[\sigma \bar{G}_j(0, 0_+)] \\ &= \sum_j J_{ij} \frac{1}{2} \sigma \langle \mathbf{S}_j \rangle \end{aligned}$$

Not shown in Fig. 1 are the self-consistent (exchange) Fock and (anomalous) Bogoliubov diagrams, which correspond to the above-mentioned flux and pairing order parameters, respectively, and do not contribute. If we assume Néel ordering in z -direction on sublattices A and B , i.e., $\langle S_A^z \rangle = -\langle S_B^z \rangle$, the self energy becomes

$$\begin{aligned} \bar{\Sigma}_A(i\omega) &= -\sigma^z m_A & \text{with } m_A = \frac{1}{2} 2dJ \langle S_A^z \rangle \\ \bar{\Sigma}_B(i\omega) &= \sigma^z m_A \end{aligned} \quad (14)$$

The coordination number $2d$ has been inserted. The Green's function (13) now reads

$$\bar{G}_A(i\omega) = \frac{i\omega - \sigma^z m_A}{(i\omega)^2 - (m_A)^2} \quad (15)$$

and similar for B with $m_A \rightarrow m_B = -m_A$. Inserting into $\langle S_A^z \rangle$ delivers the self-consistent equation for the Weiss-field m ,

$$\begin{aligned} m_A &= \frac{dJ}{2} \sum_{\alpha=\pm 1} \frac{1}{\beta} \sum_{i\omega} \frac{\alpha e^{-i\omega 0_+}}{i\omega + \alpha m_A} \\ &= \frac{dJ}{2} \tanh\left(\frac{m_A}{2T}\right) \end{aligned} \quad (16)$$

Antiferromagnetic order $m_A \neq 0$ appears below the transition temperature $T_N = \frac{d}{4}J = J/2$. The averaged local density of states of the fermions, $\rho(\omega) = \frac{1}{N_L} \sum_i \frac{1}{\pi} \text{Im} \frac{1}{2} \text{Tr} [\sigma^z \overline{G}_i(\omega - i0_+)]$, reads

$$\rho(\omega) = \frac{1}{2} [\delta(\omega - m_A) + \delta(\omega + m_A)] \quad (17)$$

The spectrum has a gap $2m_A$ as is known from the spin-density-wave state. However, our pseudo fermions do not show any dispersion, and hence $\rho(\omega)$ is δ -like. For $m_A = 0$ the bare spectrum $\rho^0(\omega) = \delta(\omega)$ is recovered.

In the ordered state $T < T_N$ the magnetic excitations should be given by spin waves. In order to compare to the results from linear spin-wave theory, we calculate the spin propagator (9) within the mean-field approximation. It is given by the RPA expression

$$\chi_{ij}^{\mu\mu'} = ([1 + J\Pi]^{-1} \Pi)_{ij}^{\mu\mu'} \quad (18)$$

with the irreducible part Π given by the fermion bubble shown in Fig. 1,

$$\Pi_i^{\mu\mu'}(i\nu) = -\frac{1}{\beta} \sum_{i\omega} \frac{1}{4} \text{Tr}[\sigma^\mu \overline{G}_i(i\omega + i\nu) \sigma^{\mu'} \overline{G}_i(i\omega)] \quad (19)$$

ν denotes a bosonic Matsubara frequency. Inserting Eq.(15) yields the transversal components

$$\Pi_A^{xx}(i\nu) = \Pi_A^{yy}(i\nu) = \frac{2m_A \langle S_A^z \rangle}{(2m_A)^2 - (i\nu)^2} \quad (20a)$$

$$\Pi_A^{xy}(i\nu) = -\Pi_A^{yx}(i\nu) = -i \frac{i\nu \langle S_A^z \rangle}{(2m_A)^2 - (i\nu)^2} \quad (20b)$$

and $\Pi_B^{xx} = \Pi_A^{xx}$, $\Pi_B^{xy} = -\Pi_A^{xy}$. The longitudinal response is exponentially small and can be ignored, $\Pi_A^{zz}, \Pi_B^{zz} \sim \exp(-\beta|m_A|)$. The susceptibility (18) is transformed into wave-vector space using

$$\chi^{\mu\mu'}(\mathbf{q}, \mathbf{q}') = \frac{1}{N_L} \sum_{i,j} \chi_{ij}^{\mu\mu'} e^{-i(\mathbf{q}\mathbf{R}_i - \mathbf{q}'\mathbf{R}_j)} \quad (21)$$

$$\Pi^{\mu\mu'}(\mathbf{q}, \mathbf{q}') = \frac{1}{N_L} \sum_i \Pi_i^{\mu\mu'} e^{-i(\mathbf{q}-\mathbf{q}')\mathbf{R}_i} \quad (22)$$

The second line leads to

$$\Pi_A^{xx}(\mathbf{q}, \mathbf{q}') = \Pi_A^{xx} \delta_{\mathbf{q}, \mathbf{q}'} \quad , \quad \Pi_A^{xy}(\mathbf{q}, \mathbf{q}') = \Pi_A^{xy} \delta_{\mathbf{q}, \mathbf{q}'} \delta_{\mathbf{q}, \mathbf{q}' \pm \mathbf{Q}}$$

with the AF ordering vector $\mathbf{Q} = (\pi, \pi, \dots)$ and $e^{\pm i\mathbf{Q}\mathbf{R}_i} = +1, -1$ for $\mathbf{R}_i \in A, B$. The interaction becomes

$$J(\mathbf{q}) = 2dJ \gamma(\mathbf{q}) \quad \text{with} \quad \gamma(\mathbf{q}) = \frac{1}{d} \sum_\mu \cos(q_\mu) \quad (23)$$

By transforming Eq.(18) in \mathbf{q} -space we find

$$\chi^{xx}(\mathbf{q}, \mathbf{q}') = \chi^{yy}(\mathbf{q}, \mathbf{q}') = \chi^{xx}(\mathbf{q}) \delta_{\mathbf{q}, \mathbf{q}'} \quad (24a)$$

$$\chi^{xy}(\mathbf{q}, \mathbf{q}') = -\chi^{yx}(\mathbf{q}, \mathbf{q}') = \chi^{xy}(\mathbf{q}) \delta_{\mathbf{q}, \mathbf{q}' \pm \mathbf{Q}} \quad (24b)$$

and Eq.(18) takes the form (omitting the \mathbf{q} arguments)

$$\begin{pmatrix} (1 + J\Pi_A^{xx}) & J\Pi_A^{xy} \\ J\Pi_A^{xy} & (1 - J\Pi_A^{xx}) \end{pmatrix} \begin{pmatrix} \chi^{xx} \\ \chi^{xy} \end{pmatrix} = \begin{pmatrix} \Pi_A^{xx} \\ \Pi_A^{xy} \end{pmatrix}$$

Using Eqs.(20), (23), (14) with $J(\mathbf{q} \pm \mathbf{Q}) = -J(\mathbf{q})$ gives

$$\chi^{xx}(\mathbf{q}, i\nu) = 2dJ(\langle S_A^z \rangle)^2 \frac{1 - \gamma(\mathbf{q})}{\Omega^2(\mathbf{q}) - (i\nu)^2} \quad (25a)$$

$$\chi^{xy}(\mathbf{q}, i\nu) = -i \langle S_A^z \rangle \frac{i\nu}{\Omega^2(\mathbf{q}) - (i\nu)^2} \quad (25b)$$

These response functions have poles at $\pm \Omega(\mathbf{q})$,

$$\Omega(\mathbf{q}) = 2dJ |\langle S_A^z \rangle| \sqrt{1 - \gamma^2(\mathbf{q})} \simeq c_0 |\mathbf{q} - \mathbf{Q}| \quad (26)$$

$\Omega(\mathbf{q})$ resembles the magnon dispersion from linear spin-wave theory³⁹ (SWT). At low energy it has two branches with linear dispersion for $\mathbf{q} \simeq 0$ and $\mathbf{q} \simeq \mathbf{Q}$. For $T \ll T_N$ the spin-wave velocity c_0 is temperature independent (up to exponentially small terms) and given by

$$c_0 = 2\sqrt{d}J |\langle S_A^z \rangle| \simeq 2\sqrt{d}J S = \sqrt{2}J$$

This also reproduces exactly the result from SWT. The response function measured in neutron-scattering experiments is $\chi''(\mathbf{q}, \omega) = \text{Im} \chi^{xx}(\mathbf{q}, \omega + i0_+)$ and comes out from Eq.(25a) as

$$\begin{aligned} \chi''(\mathbf{q}, \omega) &= \frac{\pi}{2} |\langle S_A^z \rangle| \frac{1 - \gamma(\mathbf{q})}{\sqrt{1 - \gamma^2(\mathbf{q})}} \times \\ &\quad \times [\delta(\omega - \Omega(\mathbf{q})) - \delta(\omega + \Omega(\mathbf{q}))] \end{aligned} \quad (27)$$

The spin-wave excitations remain undamped (δ -like) throughout the whole Brillouin zone, since $\max(\Omega(\mathbf{q})) = 2dJ|\langle S_A^z \rangle| = 2|m_A|$ at the magnetic zone boundary just reaches the gap $2|m_A|$ for charge fluctuations of the auxiliary fermions. The spectral weight of the magnons is measured by the transversal static structure factor $S^\perp(\mathbf{q}, \mathbf{q}') = \langle S_{\mathbf{q}}^x S_{-\mathbf{q}'}^x \rangle = S^\perp(\mathbf{q}) \delta_{\mathbf{q}, \mathbf{q}'}$ with

$$\begin{aligned} S^\perp(\mathbf{q}) &= \frac{1}{\pi} \int_{-\infty}^{\infty} d\omega [1 + g(\omega)] \chi''(\mathbf{q}, \omega) \\ &= \frac{|\langle S_A^z \rangle|}{2} \coth\left(\frac{\Omega(\mathbf{q})}{2T}\right) \frac{1 - \gamma(\mathbf{q})}{\sqrt{1 - \gamma^2(\mathbf{q})}} \end{aligned} \quad (28)$$

$g(\omega)$ denotes the Bose function. Eqs.(27), (28) result from mean-field theory and apply to any dimension $d \geq 1$. At zero temperature $|\langle S_A^z \rangle| \coth(.)/2 \rightarrow 1/4$, and $S^\perp(\mathbf{q})$ becomes identical to SWT.

B. $1/S$ Corrections

The mean-field theory presented above can be obtained as the first approximation in an expansion in $1/S$. Following Refs. 60,61,62 the fermion is decorated with an additional ‘orbital’ quantum number κ , $f_{i\alpha} \rightarrow f_{i\alpha\kappa}$, with

$\kappa = 1, 2, \dots, N_S$, $N_S = S + 1/2$ for half-integer spin S . On each lattice site i there are now $2N_S = (2S+1)$ states available. An expansion in $1/N_S \sim 1/S$ is performed by re-scaling the interaction $J \rightarrow J = \tilde{J}/N_S$ with $\tilde{J} = \text{const.}$ in each diagram and in Eq.(18), and counting a prefactor N_S for each closed fermion loop. The limit $N_S \rightarrow \infty$ then produces the mean-field approximation.

To complete the comparison of the auxiliary-fermion approach to spin-wave theory we also sketch the calculation of the first correction $\sim 1/N_S$ to the staggered magnetization, $\langle S_i^z \rangle = \langle S_i^z \rangle^{\text{MF}} + \Delta \langle S_i^z \rangle$. Note that $\langle S_i^z \rangle^{\text{MF}} \sim (1/N_S)^0$. The $1/N_S$ -correction is shown in Fig. 1 and reads

$$\Delta \langle S_i^z \rangle = \frac{1}{2^3 \beta^2} \sum_{i\nu, i\omega} \sum_{\mu, \mu'} D_i^{\mu\mu'}(i\nu) \times \text{Tr}[\sigma^z \bar{G}_i(i\omega) \sigma^\mu \bar{G}_i(i\omega + i\nu) \sigma^{\mu'} G_i(i\omega)] \quad (29)$$

where we already returned to the physical case $S = 1/2 \leftrightarrow N_S = 1, \tilde{J} = J$. The renormalized spin interaction has been introduced,

$$D_{ij}^{\mu\mu'}(i\nu) = -J_{ij} + \sum_{l,k} J_{il} \chi_{lk}^{\mu\mu'}(i\nu) J_{kj} \quad (30)$$

The local $D_i \equiv D_{ii}$ appearing in Eq.(29) has no contribution from the bare interaction, since $J_{ii} = 0$. However, propagating spin excitations described by the susceptibility χ_{lk} contribute to D_i . With Eq.(21) it follows

$$D_i^{\mu\mu'}(i\nu) = \frac{1}{N_L} \sum_{\mathbf{q}, \mathbf{q}'} J(\mathbf{q}) \chi^{\mu\mu'}(\mathbf{q}, \mathbf{q}') \times \text{Tr}[\sigma^z \bar{G}_i(i\omega) \sigma^\mu \bar{G}_i(i\omega + i\nu) \sigma^{\mu'} G_i(i\omega)] \quad (31)$$

Eq.(29) becomes for the A -sublattice, with the fermion propagator (15) inserted,

$$\Delta \langle S_A^z \rangle = \frac{1}{4\beta^2} \sum_{i\omega, i\nu} \sum_{\alpha=\pm 1} \times \frac{\alpha D_A^{xx}(i\nu) + i D_A^{xy}(i\nu)}{(i\omega + \alpha m_A)^2 (i\omega + i\nu - \alpha m_A)} \quad (32)$$

$\chi^{yy} = \chi^{xx}$ and $\chi^{yz} = -\chi^{xy}$ have been utilized. The longitudinal $D^{zz} \sim \Pi^{zz}$ has vanishing weight and does not contribute. The transversal components read with Eq.(31) and the relations given in the text below Eq.(21):

$$D_A^{xx}(i\nu) = \frac{1}{N_L} \sum_{\mathbf{q}} J^2(\mathbf{q}) \chi^{xx}(\mathbf{q}, i\nu)$$

$$D_A^{xy}(i\nu) = -\frac{1}{N_L} \sum_{\mathbf{q}} J^2(\mathbf{q}) \chi^{xy}(\mathbf{q}, i\nu)$$

$D_B^{xx} = D_A^{xx}$, $D_B^{xy} = -D_A^{xy}$ on the B -sublattice. These are inserted into Eq.(32), using the mean-field expressions (25) for the susceptibilities. Furthermore Eq.(23) and $\sum_{\mathbf{q}} \gamma(\mathbf{q}) = 0$ are taken into account, turning Eq.(32)

into an expression where the sums over fermionic (ω) and bosonic (ν) Matsubara frequencies still have to be performed. This is done with

$$\frac{1}{\beta} \sum_{i\omega} \mathcal{F}(i\omega) = \oint \frac{dz}{2\pi i} f(z) \mathcal{F}(z)$$

$$\frac{1}{\beta} \sum_{i\nu} \mathcal{B}(i\nu) = -\frac{1}{2} \oint \frac{dz}{2\pi i} \coth(\beta z/2) \mathcal{B}(z)$$

$f(z)$ denotes the Fermi function, and the contour encircles the real axis, where $\mathcal{F}(z), \mathcal{B}(z)$ may be non-analytic. At low temperature $\beta |m_A| \gg 1$ the result is

$$\Delta |\langle S_A^z \rangle| = -\frac{\epsilon}{2S} \quad (33)$$

$$\epsilon = \frac{1}{2N_L} \sum_{\mathbf{q}} \left[\frac{\coth(\frac{\Omega(\mathbf{q})}{2T})}{\sqrt{1 - \gamma^2(\mathbf{q})}} - 1 \right]$$

In the ground state at $T = 0$, where $\coth(\Omega/2T) \rightarrow 1$, Eq.(33) represents the reduction of the staggered magnetization due to quantum fluctuations. It resembles exactly the $1/S$ -correction known from SWT. In 2 dimensions it is finite, with the numerical value $\Delta |\langle S_A^z \rangle| = -\epsilon = -0.197$, i.e., for $\langle S^z \rangle > 0$ we have $[\langle S^z \rangle + \Delta \langle S^z \rangle]/\langle S^z \rangle \simeq 0.61$. At $T > 0$, however, the diverging number of thermally excited magnons with low energies destroy magnetic order in 2 dimensions (theorem of Mermin and Wagner): From Eq.(33) we get for wave vectors \mathbf{q} close to 0 or \mathbf{Q} , where $\Omega(\mathbf{q}) < T$ and the thermal prefactor $\coth(\Omega/2T) \simeq 2T/\Omega$,

$$T > 0 : \Delta \langle S_A^z \rangle \sim \frac{T}{SJ} \int \frac{d^d k}{k^2} + \text{reg.}$$

The integral diverges in the infrared $k \rightarrow 0$ for $d < 3$, indicating the well-known breakdown of perturbation theory at any finite T .

IV. SELF-CONSISTENT APPROXIMATION FOR FINITE TEMPERATURE IN 2D

In order to fulfill Mermin-Wagner's theorem, i.e., to suppress the mean-field transition temperature down to zero, we seek an approximation where the susceptibility χ is coupled back onto itself in a self-consistent fashion. Such an approximation has been proposed originally for the Hubbard model³³, commonly referred to as FLEX. For the present model it takes the form shown in Fig. 2. The irreducible part Π in Eq.(18) is approximated by a bubble of renormalized fermion Green's functions. The latter are in turn determined by χ through the effective interaction D , which enters the fermion's self energy in the simplest one-loop fashion. When temperature is lowered and the mean-field transition at $T \sim J$ is approached, the growing susceptibility χ should modify the

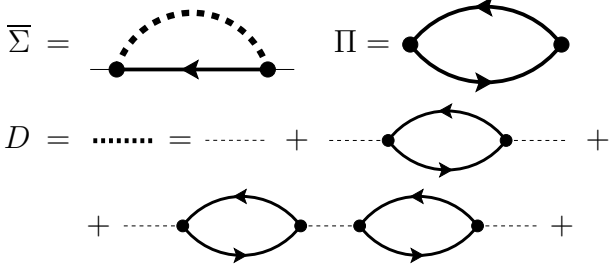


FIG. 2: The self-consistent approximation for the paramagnetic phase at $T > 0$ discussed in Sect. IV. Full lines denote the fermion propagator \bar{G} first introduced in Eq.(13), the thick dashed line is the renormalized interaction D defined in Eq.(30), the thin dashed line represents the bare interaction J . Shown are the fermion self-energy $\bar{\Sigma}$, Eq.(34), the irreducible bubble Π , Eq.(19), and the renormalized interaction D . Dots are Pauli matrices $\times 1/2$. In the paramagnetic phase the traces in spin space are easily performed, leading to the set of Eqs.(35).

spectrum of the auxiliary fermion and therefore Π , such that the increase of χ and accordingly the transition is suppressed.

The irreducible part Π and the fermion propagator \bar{G} are given by Eqs.(19) and (13), respectively. The self energy given in Fig. 2 reads

$$\bar{\Sigma}(i\omega) = \left(\frac{1}{2}\right)^2 \frac{1}{\beta} \sum_{i\nu} \sum_{\mu, \mu'} D^{\mu\mu'}(i\nu) \sigma^\mu \bar{G}(i\omega + i\nu) \sigma^{\mu'} \quad (34)$$

Without external field and in the paramagnetic phase, $\mathbf{h} = \langle \mathbf{S} \rangle = 0$, the fermions are spin degenerate, $\bar{G} = \sigma^0 G$, $\bar{\Sigma} = \sigma^0 \Sigma$, and the response becomes isotropic, $\Pi^{\mu\mu'} = \delta_{\mu\mu'} \Pi$. Equations (13), (18), (19), (30), (34) now simplify to

$$\Pi(i\nu) = -\frac{1}{2\beta} \sum_{i\omega} G(i\omega + i\nu) G(i\omega) \quad (35a)$$

$$\chi(\mathbf{q}, i\nu) = \frac{\Pi(i\nu)}{1 + J(\mathbf{q})\Pi(i\nu)} \quad (35b)$$

$$D(i\nu) = \frac{1}{N_L} \sum_{\mathbf{q}} J^2(\mathbf{q}) \chi(\mathbf{q}, i\nu) \quad (35c)$$

$$\Sigma(i\omega) = \frac{3}{4\beta} \sum_{i\nu} D(i\nu) G(i\nu + i\omega) \quad (35d)$$

$$G(i\omega) = [i\omega - \Sigma(i\omega)]^{-1} \quad (35e)$$

Note that the first bare J to D in Fig. 2 does not contribute, since $J_{ii} = 0$ or equivalently $\sum_{\mathbf{q}} J(\mathbf{q}) = 0$.

It has been emphasized above that the non-local expectation values $\langle f_{i\alpha}^\dagger f_{j\alpha} \rangle$ and $\langle f_{i\uparrow}^\dagger f_{j\downarrow} \rangle$ are zero at 1/2 filling. Therefore the pseudo fermions do not show any dispersion, hence the fermion propagator $G_{ij} = \delta_{ij} G_i$, $G_i = G$ and the bubble $\Pi_{ij} = \delta_{ij} \Pi_i$, $\Pi_i = \Pi$ are local, i.e., wave-vector independent. The susceptibility $\chi(\mathbf{q})$,

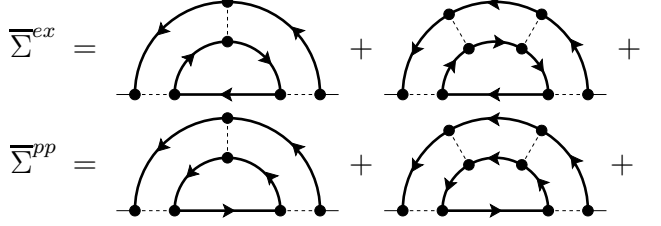


FIG. 3: Self-energy diagrams of ladder type for the exchange particle-hole ('RVB/flux') channel (top row) and the particle-particle (pairing) channel (bottom row). The contribution of $\bar{\Sigma}^{ex}$ and $\bar{\Sigma}^{pp}$ has almost no effect on the results, see text, Sect. IV.

however, is \mathbf{q} -dependent through the Heisenberg interaction $J(\mathbf{q}) = 2dJ\gamma(\mathbf{q})$ occurring in Eq.(35b). The latter has been introduced in Eq.(23). However, the argument for the fermions being local is based on mean-field theory. If fluctuations are included in the fermion self-energy, the ladder-diagram series shown in Fig. 3 should also be taken into account. While $\bar{\Sigma}$ in Fig. 2 captures the effect of magnetic fluctuations on the fermions, $\bar{\Sigma}^{ex}$ and $\bar{\Sigma}^{pp}$ contain fluctuations in the 'RVB/flux' channel and the pairing channel, respectively: A large numerical contribution from $\bar{\Sigma}^{ex}$ would indicate a close-by instability to a flux phase ($\langle f_i^\dagger f_j \rangle \neq 0$), whereas $\bar{\Sigma}^{pp}$ would dominate if the pseudo fermions were instable to pairing ($\langle f_i f_j \rangle \neq 0$). In the 1/2-filled case considered in this paper, both $\bar{\Sigma}^{ex/pp}$ are numerically equivalent by particle-hole symmetry. The numerical calculation presented in Sect. IV B has been repeated with the two extra channels from Fig. 3 included. Even at the lowest temperature reached the results where merely altered quantitatively; numbers reported in Sect. IV B came out different by $\simeq 20\%$. The ladder sums (susceptibilities) appearing in $\bar{\Sigma}^{ex/pp}$ remain small, i.e., $\sim 1/J$. Apparently, the self energies from Fig. 3 can be omitted and will no longer be considered.

In the following we calculate the antiferromagnetic correlation length $\xi(T)$ and the spectrum $S(\mathbf{q}, \omega)$ of magnetic fluctuations from Eqs.(35).

A. Static Approximation: Correlation Length, Energy Scale, Dynamical Scaling

In order to proceed by analytical calculation we approximate the effective interaction D in the self energy Eq.(35d) by its static value, $D(i\nu) = D(0)\delta_{\nu,0}$. This static (classical) approximation should be reasonable if the characteristic energy ω_0 of spin fluctuations is small compared to temperature. This is the result of earlier studies mentioned in the introductory Sect. I and will also come out of the following calculation as well as the numerical solution presented in Sect. IV B below.

With $D(i\nu) = D(0)\delta_{\nu,0}$ Eq.(35d) turns into

$$\Sigma(i\omega) = \frac{3}{4\beta}D(0)G(i\omega) = \left(\frac{\omega_f}{2}\right)^2 G(i\omega) \quad (36)$$

where a coupling constant $\omega_f = \sqrt{3D(0)/\beta}$ has been introduced. Eq.(35c) requires the static susceptibility $\chi(\mathbf{q}, 0)$. At low temperature wave vectors $\mathbf{q} \simeq \mathbf{Q} \equiv (\pi, \pi)$ close to the Néel ordering-vector \mathbf{Q} give the strongest contribution, allowing to expand Eq.(23) as

$$J(\mathbf{q}) \simeq -2dJ + (\mathbf{q} - \mathbf{Q})^2 J \quad (37)$$

leading to

$$\chi(\mathbf{q}, 0) = \frac{\Pi(0)}{1 + J(\mathbf{q})\Pi(0)} \simeq \frac{1}{J} \frac{1}{\xi^{-2} + (\mathbf{q} - \mathbf{Q})^2} \quad (38)$$

where the antiferromagnetic correlation length has been identified as

$$\xi^{-2} = 2d \left(\frac{1}{2dJ\Pi(0)} - 1 \right) \quad (39)$$

The spatial dimension d has been written explicitly for clarity. In Eq.(35c) we may set $J(\mathbf{q}) \simeq J(\mathbf{Q}) = -2dJ$, and it follows for the coupling constant

$$(\omega_f)^2 = 3(2d)^2 JT \int \frac{d^d k}{(2\pi)^d} \frac{1}{\xi^{-2} + k^2} \quad (40)$$

In 2 dimensions this becomes

$$(\omega_f)^2 = \frac{24}{\pi} TJ \{ \ln(k_c \xi) + \mathcal{O}(\xi^{-2}) \} \quad (41)$$

where $k_c \sim 1$ denotes a wave-vector cut off coming from the Brillouin-zone boundary. In higher dimensions $d \geq 3$ we get

$$(\omega_f)^2 \sim TJ(k_c)^{d-2} \quad (42)$$

The Dyson's equation (35e) with Eq.(36) inserted reads after analytical continuation $i\omega \rightarrow z$

$$\frac{1}{G(z)} = z - \left(\frac{\omega_f}{2}\right)^2 G(z)$$

At the real axis, $z = \omega + i0_+$, this leads to

$$G(\omega + i0_+) = \frac{2\Theta(\omega_f - |\omega|)}{\omega + i\sqrt{(\omega_f)^2 - \omega^2}} + \quad (43)$$

$$+ \frac{2\Theta(|\omega| - \omega_f)}{\omega + \text{sign}(\omega)\sqrt{\omega^2 - (\omega_f)^2} + i0_+}$$

In the atomic limit $J = 0$ the spectrum of the fermions $\rho(\omega) = -\frac{1}{\pi}\text{Im}G(\omega + i0_+)$ is a delta peak at zero energy, $\rho^0(\omega) = \delta(\omega)$ from $G^0(z) = 1/z$. Through the interaction with spin fluctuations ρ is apparently broadened

into a semi-elliptic spectrum with the coupling constant ω_f appearing as a high-energy cut off: Eq.(43) gives

$$\rho(\omega) = \Theta(\omega_f - |\omega|) \frac{2}{\pi\omega_f} \sqrt{1 - (\omega/\omega_f)^2} \quad (44)$$

Eq.(44) is plotted in Fig. 5, together with the numerical solution described in Sect. IV B. In order to close the set of self-consistency equations, $\Pi(0)$ has to be calculated from Eq.(35a),

$$\Pi(0) = - \int_{-\infty}^{\infty} d\varepsilon f(\varepsilon) \rho(\varepsilon) \text{Re}G(\varepsilon) = \frac{1}{\omega_f} \Phi(T/\omega_f) \quad (45)$$

with

$$\begin{aligned} \Phi(t) &= -\frac{4}{\pi} \int_{-1}^1 dx \frac{x\sqrt{1-x^2}}{e^{x/t} + 1} \\ &= \frac{4}{3\pi} - \frac{2\pi}{3}t^2 + \mathcal{O}(t^4) \end{aligned}$$

The r.h.s. results from a Sommerfeld expansion of the integral.

When temperature is lowered in the 2D system and the correlation length ξ grows, the fermion's cut-off energy ω_f increases (see Eq.(41)), which in turn reduces the fermion spectrum $\rho(0) \sim 1/\omega_f$ and the static irreducible part $\Pi(0) \sim 1/\omega_f$. Therefore the antiferromagnetic susceptibility $\chi(\mathbf{Q}, 0) = \Pi(0)/[1 - 2dJ\Pi(0)]$ is shifted away from the critical point, and the phase transition to AF order is suppressed self-consistently. In $d \geq 3$ the correlation length ξ does not enter ω_f , Eq.(42), and this mechanism does not apply, allowing an AF transition to occur.

An explicit expression for the correlation length is obtained from the solution of Eqs.(39), (41), (45), omitting terms of $\mathcal{O}(\xi^{-2})$ and $\mathcal{O}(T^4)$ at low temperature. For $d = 2$ it follows from Eq.(39)

$$\Pi(0) = 1/4J + \mathcal{O}(\xi^{-2}) \quad (46)$$

This is inserted into Eq.(45), which is then solved for ω_f ,

$$\frac{\omega_f}{\omega_f^0} = 1 - \frac{\pi^2}{2} \left(\frac{T}{\omega_f^0} \right)^2 + \mathcal{O}(T^4) \quad \text{with} \quad \omega_f^0 = \frac{16J}{3\pi} \quad (47)$$

Finally, Eq.(41) gives the result $k_c \xi = \exp\{(\pi(\omega_f^0)^2)/(24TJ) + \mathcal{O}(T/J)\}$, in leading order,

$$\xi(T) \propto \exp(a_s J/T) \quad \text{with} \quad a_s = \frac{32}{27\pi} \simeq 0.38 \quad (48)$$

Accordingly the correlation length diverges exactly at $T = 0$, i.e., the Mermin-Wagner theorem is fulfilled. The exponential behavior of $\xi(T)$ is simply due to the density of states in 2D, $\mathcal{N}(\omega) = \int \frac{d^2 q}{4\pi^2} \delta(\omega - J(\mathbf{q})) \simeq \Theta(4J - |\omega|)/J$, which is constant near the band edges and therefore leads to the logarithm in Eq.(41). The correlation

length (48) is consistent with the theoretical work mentioned in Sect. I. The spin stiffness $\rho_s = a_s J / 2\pi \simeq 0.06 J$ extracted from Eq.(48) comes out too small compared to the literature, where $\rho_s \simeq 0.18$. The latter value is also the result of exact diagonalization studies in the AF ordered ground state¹ at $T = 0$.

In addition to the correlation length, the dynamics of spin fluctuations is an important issue. The damping of spin fluctuations is induced by the imaginary part of $\Pi(\omega)$, i.e., the spectrum of particle-hole excitations. From Eq.(35a) we get at $T \rightarrow 0$, with the smooth fermion spectrum (44)

$$\begin{aligned}\text{Im } \Pi(\omega + i0_+) &= \frac{\pi}{2} \int_0^\omega d\varepsilon \rho(\omega - \varepsilon) \rho(-\varepsilon) \\ &= \frac{\pi}{2} \rho(0)^2 \omega + \mathcal{O}(\omega^3)\end{aligned}$$

The real part is approximately calculated using

$$\begin{aligned}\text{Re } \Pi(\omega) &= \frac{1}{\pi} \int d\varepsilon \frac{\text{Im } \Pi(\varepsilon + i0_+)}{\varepsilon - \omega} \\ &\simeq \frac{1}{2} \rho(0)^2 \int_{-\Omega}^\Omega d\varepsilon \frac{\varepsilon}{\varepsilon - \omega}\end{aligned}$$

where a high-energy cut off $\Omega \sim J$ for spin-fluctuations has been introduced. Ω can be fixed by the condition $\text{Re } \Pi(0) = \Pi(0)$, and it follows

$$\text{Re } \Pi(\omega) = \Pi(0) \left[1 - (\omega/\Omega)^2 \right] + \mathcal{O}(\omega^4)$$

with $\Omega = \Pi(0)/\rho(0)^2 = \frac{16}{9}J$. Here $\Pi(0) = 1/4J$ and $\rho(0) = 1/\pi\omega_f^0 = 3/16J$ from Eqs.(44), (46) have been used. The susceptibility Eq.(35b) at the real axis $i\nu \rightarrow \omega + i0_+$ becomes

$$\begin{aligned}\chi(\mathbf{q}, \omega)^{-1} &= \Pi(\omega + i0_+)^{-1} + J(\mathbf{q}) \\ &= \frac{1}{\chi(\mathbf{q})} - \frac{1}{\Pi(0)} \left[i \frac{\pi}{2} \left(\frac{\omega}{\Omega} \right) + \right. \\ &\quad \left. + \left(\frac{\pi^2}{4} - 1 \right) \left(\frac{\omega}{\Omega} \right)^2 \right] + \mathcal{O}(\omega^3)\end{aligned}$$

with the static susceptibility $\chi(\mathbf{q})$ stated in Eq.(38). Introducing a spin-wave velocity c and -damping constant γ ,

$$c^2 = \frac{4\Pi(0) J \Omega^2}{\pi^2 - 4} \simeq (1.47 J)^2, \quad \gamma = \frac{2\pi \Omega}{\pi^4 - 4} \simeq 1.90 J$$

the dynamical susceptibility takes the familiar form

$$\chi(\mathbf{q}, \omega) = \frac{c^2}{J} \left[c^2(k^2 + \xi^{-2}) - \omega^2 - i\gamma\omega \right]^{-1} \quad (49)$$

where $\mathbf{k} = (\mathbf{q} - \mathbf{Q})$.

The calculation seems to yield spin-wave like excitations for wave vectors $k \gg \xi^{-1}$ far enough off the Néel

vector \mathbf{Q} , with the familiar dispersion $\Omega(\mathbf{q}) = ck$. However, the damping γ appears much larger than the spin-wave energy, i.e., the ‘spin waves’ are totally overdamped: For wave vectors well inside the 1. B.Z., $k \ll 1$, it is $|\omega| \simeq \Omega(\mathbf{q}) \sim Jk \ll J$ and thus $\gamma \gg |\omega|$. Therefore the ω^2 in Eq.(49) may be omitted, leading to

$$\chi(\mathbf{q}, \omega) = \chi(\mathbf{q}) \frac{i\Gamma(\mathbf{q})}{\omega + i\Gamma(\mathbf{q})}, \quad \Gamma(\mathbf{q}) = \frac{1}{\chi(\mathbf{q})} \frac{c^2}{\gamma J} \quad (50)$$

The dynamical structure factor

$$S(\mathbf{q}, \omega) = \frac{\text{Im } \chi(\mathbf{q}, \omega)}{1 - e^{-\beta\omega}} \simeq \frac{T}{\omega} \text{Im } \chi(\mathbf{q}, \omega) \quad (51)$$

shows a single relaxation-like peak at $\omega = 0$. At long wavelengths $k \ll \xi^{-1}$ the half-linewidth of this peak is $\Gamma(\mathbf{q}) \propto \Gamma(\mathbf{Q}) \sim J\xi^{-2}$, which turns to zero as the AF transition is reached (critical slowing down), with the dynamical exponent $z = 2$. This is compatible with hydrodynamic theory⁶³ and the studies of $S(\mathbf{q}, \omega)$ referenced in Sect. I. Our result $z = 2$, however, differs from the $z = 1$ found in these studies. At short wavelengths, $k \gg \xi^{-1}$, the structure factor still consists of a single peak at $\omega = 0$, with a k -dependent linewidth $\Gamma(\mathbf{q}) \sim Jk^2$. This is in strong contradiction to the above-mentioned theories, where for $k \gg \xi^{-1}$ the structure factor features two peaks with some dispersion $\omega = \pm\Omega(\mathbf{q})$ and finite width. These peaks are interpreted as spin-wave like excitations, visible only at short enough wavelengths $\ll \xi$.

Since the ω^2 -term in Eq.(49) does not contribute, the dynamical scaling property (3), (4) is almost trivially fulfilled: From Eqs.(49), (51) it follows $S(\mathbf{q}, \omega) = \frac{T\xi^2}{\omega J} \text{Im} [1 + (k\xi)^2 - i(\omega/\omega_0)]^{-1}$, with the energy scale

$$\omega_0 = \Gamma(\mathbf{Q}) = \frac{c^2}{\gamma\xi^2} \propto J\xi^{-2} \quad (52)$$

The static structure factor results from $S^{st}(\mathbf{q}) = \frac{1}{\pi} \int d\omega S(\mathbf{q}, \omega) \simeq T\chi(\mathbf{q}, 0) = \frac{T\xi^2}{J} [1 + (k\xi)^2]^{-1}$, reproducing Eqs.(3), (4) with the scaling functions

$$\varphi(x) = \frac{1}{1 + x^2}, \quad \Phi(x, y) = \frac{1 + x^2}{(1 + x^2)^2 + y^2} \quad (53)$$

For any fixed wave vector $x = k\xi$ the ‘shape function’ $\Phi(x, y)$, $y = \omega/\omega_0$ is a simple Lorentzian located at $\omega = 0$, normalized to $\Phi(0, 0) = 1$. The inset of Fig. 4 shows Φ from Eq.(53), the main figure the corresponding result from the numerical solution to be described below.

B. Numerical Results

So far we have considered a static approximation, where the susceptibility Eq.(35b) has been taken in the classical limit, $\chi(\mathbf{q}, i\nu) = \chi(\mathbf{q}, 0)\delta_{\nu,0}$ inside the effective local interaction D , Eq.(35c). The set of equations (35)

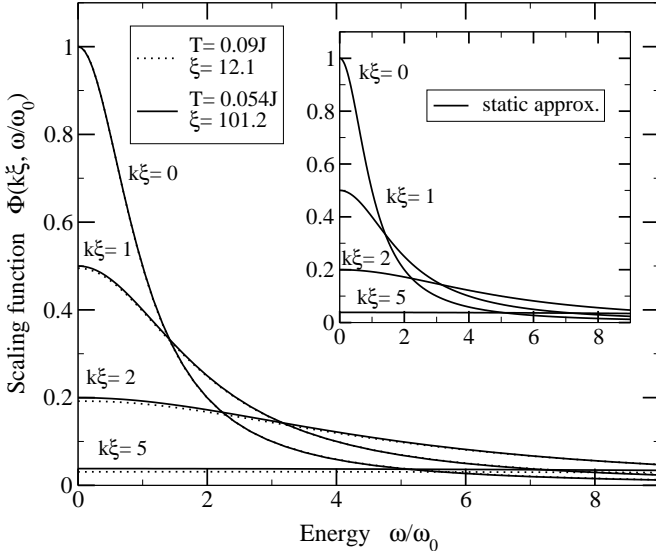


FIG. 4: **Main figure:** Dynamical structure factor from the numerical solution of the self-consistent approximation Eqs.(35). Plotted is the scaling function $\Phi(k\xi, \omega/\omega_0)$ at low energies $\sim \omega_0$. Φ is shown for fixed wave vectors $k = 0, \xi^{-1}, 2\xi^{-1}, 5\xi^{-1}$, each for 2 different temperatures corresponding to the correlation lengths $\xi = 12.1, 101.2$. The curves lie almost on top of each other, indicating that dynamical scaling holds for $\xi > 10$. **Inset:** Analytically calculated scaling function $\Phi(k\xi, \omega/\omega_0)$, Eq.(53), from the static approximation.

has also been solved numerically with all frequency dependencies taken into account. Eqs.(35) are re-written at the real axis, see Eq.(A1) in Appendix A 1, and solved by numerical iteration. A stable solution is obtained for temperatures $0.5J \geq T \geq 0.054J$, corresponding to a correlation length $0.7 \leq \xi \leq 101$, in units of the lattice spacing. ξ is extracted from the static susceptibility at $\mathbf{q} = \mathbf{Q}$ using Eq.(39), it is well reproduced by $\xi(T) = \text{const.} \times \exp(aJ/T)$ with $a = 0.30$. The fit of the numerical data $\xi(T)$ is performed by a linear regression of $[t \ln(\xi)]$ to the function $[a + t \ln(\text{const.})]$, $t = T/J$. The exponent $a_s = 0.38$ from the static approximation, Eq.(48), almost agrees with the numerical result.

The numerical solution is also consistent with the dynamical scaling hypothesis: If the static scaling function $\varphi(x) = S^{st}(\mathbf{q})/S^{st}(\mathbf{Q})$ is plotted against $x = k\xi$, curves lie on top of each other for temperatures $T < 0.1J$ where $\xi > 10$. $\varphi(x)$ is well described by the simple Lorentzian shape (53) of the static approximation. The energy scale ω_0 is extracted from the numerical output via

$$\omega_0 = \frac{S^{st}(\mathbf{q} = \mathbf{Q})}{S(\mathbf{q} = \mathbf{Q}, \omega = 0)} \quad (54)$$

which gives ω_0 up to a constant prefactor, which is chosen such that $\Phi(0, 0) = 1$. The scaling function $\Phi(x, y)$ is then gained from

$$\Phi(x, y) = \omega_0 S(\mathbf{q}, \omega) / S^{st}(\mathbf{q}) \quad (55)$$

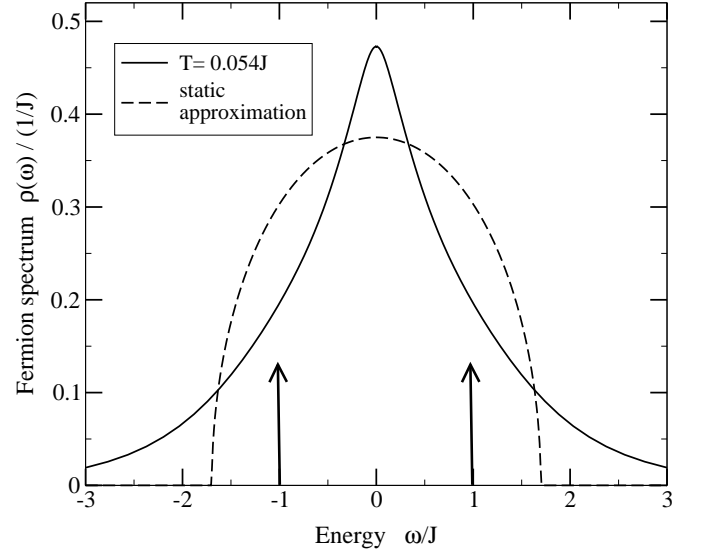


FIG. 5: Spectral function $\rho(\omega)$ of the fermion propagator Eq.(35e). Full line: numerical solution of Eqs.(35). Dashed line: static approximation, Eq.(44). The arrows indicate delta peaks, representing $\rho(\omega)$ in the antiferromagnetic phase at $T = 0$ in mean-field theory, Eq.(17).

and plotted against $x = k\xi$, $y = \omega/\omega_0$. Fig. 4 shows $\Phi(x, y)$ for two temperatures, where $\xi \geq 10$. Apparently scaling is well obeyed, and the shape of Φ agrees with the static approximation. In particular, it consists of a single peak even for $k\xi > 1$. In Sect. V a modified self-consistent approximation will be presented, where $\Phi(x, y)$ features spin-wave like propagating excitations for $k\xi > 1$; also the dynamical exponent will come out correctly as $z = 1$.

For completeness the spectrum $\rho(\omega)$ of auxiliary fermions is shown in Fig. 5. The delta-peak of the bare ($J = 0$) fermion is broadened into a continuum of width $\sim 2J$, qualitatively similar to the static approximation, Eq.(44). Further comments on $\rho(\omega)$ will be made in Sect. IV D.

C. Conserving-Approximation Approach: Vertex Corrections

We now turn to the so-called conserving-approximation method, which has been left aside so far: The spin susceptibility (9) is given by

$$\hat{\chi}_{ij}^{\mu\mu'}(\tau, \tau') = \frac{\delta \langle S_i^\mu(\tau) \rangle}{\delta h_j^{\mu'}(\tau')} \bigg|_{\mathbf{h}=0} = \frac{-\delta^2 W[\mathbf{h}]}{\delta h_i^\mu(\tau) \delta h_j^{\mu'}(\tau')} \bigg|_{\mathbf{h}=0}$$

$\mu, \mu' = x, y, z$. h^μ are the components of the magnetic source field \mathbf{h} . W is the generating functional (free energy) $W[T, \mathbf{h}] = -\ln \int \mathcal{D}[f, \bar{f}] e^{-A}$ to be calculated from the action (8) of the model. W can be expressed as a functional^{64,65} of G and Σ , $W[T, \mathbf{h}] = \Phi[G] - 2\text{Tr}[\Sigma G] - 2\text{Tr} \ln[-G_0^{-1} + \Sigma]$. The functional $\Phi[G]$

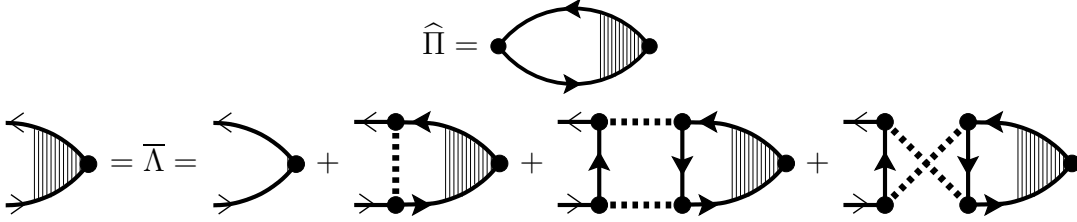


FIG. 6: **Top:** Irreducible bubble $\widehat{\Pi}$ including the vertex corrections from the conserving approximation-scheme. **Bottom:** Bethe-Salpeter equation for the vertex function $\overline{\Lambda}$. Lines are those introduced in Fig. 2, calculated self-consistently from the corresponding equations (35).

appearing here is related to the fermion self-energy via $\Sigma[G] = \frac{1}{2}\delta\Phi/\delta G$. The existence of a Φ -functional for a particular approximation of Σ is a sufficient condition for $\widehat{\chi}$ to respect conservation laws^{64,66}. The self-energy in Fig. 2, Eq.(35) can be derived from a Φ -functional similar to the FLEX³³.

$\widehat{\chi}$ is given by the same RPA-formula (18) as χ , but the irreducible part Π from Fig. 2 has to be replaced by $\widehat{\Pi}$ shown in Fig. 6. If the theory was exact, Π and $\widehat{\Pi}$ would be identical. In any approximation, however, $\widehat{\Pi}$ contains additional vertex corrections, and $\widehat{\chi}$ differs from the correlation function χ of the self-consistency equations, e.g., Eqs.(35). If now $\widehat{\chi}$ diverges, indicating a magnetic instability at some finite temperature \widehat{T}_N in the 2D system, this is not coupled back into the self-consistency cycle. As a consequence the spurious phase transition is not suppressed, merely $\widehat{\chi}$ becomes invalid below \widehat{T}_N .

To elucidate further on this important point, we calculate the correlation length $\widehat{\xi}(T)$ from the susceptibility $\widehat{\chi}(\mathbf{q}, 0)$. We employ the static approximation described in Sect. IV A, using the fermion propagator (43) and the self-consistent D , Eq.(35c), as input. The bubble including the vertex corrections is shown in Fig. 6 and reads

$$\widehat{\Pi}_{ij}^{\mu\mu'}(i\nu) = -\frac{1}{2\beta} \sum_{i\omega} \text{Tr}[\sigma^\mu \overline{G}(i\omega + i\nu) \overline{\Lambda}_{ij}^{\mu'}(i\omega, i\nu) \overline{G}(i\omega)]$$

\overline{G} and $\overline{\Lambda}$ denote the renormalized fermion propagator and the vertex function, respectively; both are matrices in spin space. Whereas the former is always local, the latter in general depends on lattice sites i, j . In the disordered phase $\langle \mathbf{S} \rangle = 0$ we have $\overline{G} = G\sigma^0$ and $\widehat{\Pi}^{\mu\mu'} = \widehat{\Pi}^\mu \delta_{\mu\mu'}$. For the correlation length merely a knowledge of the static susceptibility is required, therefore we set $i\nu = 0$, and $\widehat{\Pi}$ reads in wave-vector space

$$\widehat{\Pi}^\mu(\mathbf{q}, 0) = -\frac{1}{\beta} \sum_{i\omega} G(i\omega)^2 \lambda^\mu(\mathbf{q}; i\omega) \quad (56)$$

$$\lambda^\mu(\mathbf{q}; i\omega) = \frac{1}{2} \text{Tr}[\sigma^\mu \overline{\Lambda}^\mu(\mathbf{q}; i\omega)]$$

The Bethe-Salpeter equation for $\overline{\Lambda}$ is depicted in Fig. 6,

for $i\nu = 0$ it takes the form

$$\begin{aligned} \overline{\Lambda}^\mu(\mathbf{q}; i\omega) = & \frac{1}{2} \sigma^\mu + \\ & + \frac{1}{4} \frac{1}{\beta} D(0) G(i\omega)^2 \sum_{\tilde{\mu}=x,y,z} \sigma^{\tilde{\mu}} \overline{\Lambda}^\mu(\mathbf{q}; i\omega) \sigma^{\tilde{\mu}} - \\ & - \frac{1}{16} \frac{1}{N_L} \sum_{\mathbf{k}} \frac{1}{\beta} D(\mathbf{k} + \mathbf{q}, 0) D(\mathbf{k}, 0) G(i\omega)^2 \times \\ & \times \sum_{\tilde{\mu}, \tilde{\mu}'} (\sigma^{\tilde{\mu}} \sigma^{\tilde{\mu}'} + \sigma^{\tilde{\mu}'} \sigma^{\tilde{\mu}}) \times \\ & \times \frac{1}{\beta} \sum_{i\tilde{\omega}} G(i\tilde{\omega})^3 \text{Tr}[\sigma^{\tilde{\mu}} \overline{\Lambda}^\mu(\mathbf{q}; i\tilde{\omega}) \sigma^{\tilde{\mu}'}] \end{aligned}$$

$D(\mathbf{k}, i\nu)$ denotes the renormalized interaction Eq.(30) and $D(i\nu)$ its local version Eq.(35c). In the static approximation we have used $D(i\nu) = D(0)\delta_{\nu,0}$. The last term in the equation above corresponds to the last two diagrams in Fig. 6. In the static case $i\nu = 0$ considered here, these diagrams cancel, since $(\sigma^{\tilde{\mu}} \sigma^{\tilde{\mu}'} + \sigma^{\tilde{\mu}'} \sigma^{\tilde{\mu}}) = 2\sigma^0 \delta_{\tilde{\mu}, \tilde{\mu}'}$, and therefore their contribution to λ^μ is $\propto \text{Tr}[\sigma^0 \sigma^0] = 0$. In addition, in the undoped case of the Heisenberg model it is $\sum_{i\tilde{\omega}} G(i\tilde{\omega})^l = 0$, $l = 3, 5, 7, \dots$, due to particle-hole symmetry. Thus only the first two terms in $\overline{\Lambda}$ contribute, giving the local vertex function

$$\lambda^\mu(\mathbf{q}; i\omega) = \frac{1}{2} - \frac{1}{4\beta} D(0) G(i\omega)^2 \lambda^\mu(\mathbf{q}; i\omega) \quad (57)$$

We used $\text{Tr}[\sigma^{\tilde{\mu}} \sigma^\mu \sigma^{\tilde{\mu}} \overline{\Lambda}^\mu] = (\pm) \text{Tr}[\sigma^\mu \Lambda^\mu]$ with $(+)$ for $\tilde{\mu} = \mu$ and $(-)$ for $\tilde{\mu} \neq \mu$. From Eqs.(57) and (56) it follows $\widehat{\Pi}(0) = \widehat{\Pi}^\mu(\mathbf{q}, 0)$,

$$\widehat{\Pi}(0) = \frac{1}{2\pi} \int d\varepsilon f(\varepsilon) \text{Im} \frac{1}{G(\varepsilon + i0_+)^{-2} + \frac{1}{3}(\omega_f/2)^2}$$

with the coupling constant $\omega_f = \sqrt{3D(0)/\beta}$ introduced below Eq.(36). For the fermion propagator G the self-consistent solution Eq.(43) has to be inserted, with the result

$$\begin{aligned} \widehat{\Pi}(0) &= \frac{1}{\omega_f} \widehat{\Phi}(T/\omega_f) \\ \widehat{\Phi}(t) &= -\frac{3}{\pi} \int_{-1}^1 dx \frac{x\sqrt{1-x^2}}{x^2 + 1/3} \frac{1}{e^{x/t} + 1} \\ &= \widehat{\Phi}(0) - \frac{3\pi}{2} t^2 + \mathcal{O}(t^4) \end{aligned} \quad (58)$$

and $\widehat{\Phi}(0) \simeq 0.497$. With the T -dependent cut off ω_f from Eq.(47), the vertex-renormalized bubble becomes

$$\begin{aligned}\widehat{\Pi}(0) &= \frac{1}{\omega_f^0} \left[\widehat{\Phi}(0) - (T/\omega_f^0)^2 \frac{\pi}{2} (3 - \pi \widehat{\Phi}(0)) \right] + \mathcal{O}(T^4) \\ &= \frac{1}{J} [(0.293) - (0.462) (T/J)^2]\end{aligned}$$

Now the static susceptibility $\widehat{\chi}$ is formed similar to Eq.(38), and the corresponding correlation length is given by $\widehat{\xi}^2 = J\widehat{\chi}(\mathbf{Q}, 0) = J\widehat{\Pi}(0) / (1 - 2dJ\widehat{\Pi}(0))$, leading to

$$\widehat{\xi}(T) \sim \left(\frac{\widehat{T}_N}{T - \widehat{T}_N} \right)^{1/2} \quad \text{with} \quad \widehat{T}_N = (0.305) J \quad (59)$$

The spin susceptibility $\widehat{\chi}$ derived from the conserving-approximation principle contains a spurious transition to AF magnetic order at some finite temperature $\widehat{T}_N \simeq 0.3 J$. The mean-field transition $T_N = 0.5 J$ is only slightly suppressed. Close to \widehat{T}_N the correlation length $\widehat{\xi}$ shows a mean-field like behavior, rather than the exponential one of the 2D system. The vertex corrections included in $\widehat{\Pi}$ apparently have a dramatic effect: $\Pi(0)$, the irreducible bubble entering Eqs.(35), is forced by self-consistency to be constant, $J(\mathbf{Q})\Pi(0) = (-1) + \mathcal{O}(e^{-J/T})$, see Eq.(46). Accordingly the fermion cut-off ω_f , Eq.(47), comes out such that this $\Pi(0)$ is reproduced if ω_f is inserted into Eq.(45), in particular the T -dependence of ω_f cancels the one from $\Phi(t)$, up to terms $\mathcal{O}(e^{-J/T})$. However, if the same ω_f is inserted into $\widehat{\Pi}(0)$, Eq.(58), this cancellation no longer takes place, leading to the qualitatively different result for $\widehat{\xi}$ compared to ξ .

In conclusion, the susceptibility derived from the principle of conserving approximation leads to very unsatisfactory results. It is expected that the striking difference between ξ and $\widehat{\xi}$ is not overcome if a more sophisticated approximation for the self-consistent $\Pi(0)$ is used, since again $\widehat{\Pi}$ will differ from Π . Therefore we will drop the conserving-approximation scheme in the following and take the self-consistent correlation function χ also as an approximation for the spin susceptibility, $\widehat{\chi} := \chi$. Since the sufficient condition for $\widehat{\chi}$ to respect conservation laws is now lost, this issue has to be discussed separately.

D. Absence of Short-Range Order: Overdamping

It has been demonstrated that a self-consistent approximation, constructed in close analogy to FLEX, provides the required suppression of the mean-field transition temperature $T_N \rightarrow 0$ in two dimensions. The correlation length $\xi(T)$ came out qualitatively correct. The dynamics of spin fluctuations is governed by an energy scale ω_0 that obeys critical slowing down. However, the dynamical exponent $z = 2$ is inconsistent with known results for the 2D Heisenberg model and the QNL σ M. Also the dynamical structure factor $S(\mathbf{q}, \omega)$ does not show any

damped spin-wave peaks expected at wave vectors far off the Néel vector $\mathbf{Q} = (\pi, \pi)$.

The lack of peak dispersion in S can be traced back to the fermion density of states $\rho(\omega)$, displayed in Fig. 5. There is no sign of a suppression around $\omega = 0$ even as $T \rightarrow 0$ and therefore any magnons are completely damped out. In the AF ordered state at $T = 0$ the fermion's spectrum must show some sort of (pseudo) gap, allowing for well defined spin waves. In mean-field theory, there is even a true gap, see Eq.(17). In the following section a modified (actually simplified) approximation will be discussed, where a pseudo-gap like suppression around $\omega = 0$ is observed in $\rho(\omega)$ at low temperature. In that approximation the spin dynamics come out quite satisfactorily.

V. MINIMAL SELF-CONSISTENT APPROXIMATION (MSCA) FOR $T > 0$

The most important property of the approximation discussed above is the self-consistent treatment of the susceptibility χ . This was achieved by renormalizing the propagator G of the fermion self-consistently, with χ appearing in the self energy to 1-loop order, see Fig. 2. In that scheme, the fermion propagator is subject to a self-consistency loop even for fixed χ , which smears any pole structures, leading to a smooth spectrum $\rho(\omega)$. Fig. 7 shows an approximation with a minimal amount of self-consistency, which we refer to as the ‘minimal self-consistent approximation’ (MSCA). In Fig. 7 only the susceptibility (the bubble series entering D) is a self-consistent quantity. The auxiliary-fermion propagator, which is itself not a physical object, is kept unrenormalized. The Π shown in Fig. 7 is a bubble of bare fermions, with $D \sim \chi$ inserted to infinite order in the simplest way that preserves the analytic properties of $\Pi(z)$.

The set of equations corresponding to Fig. 7 actually is a simplification of Eqs.(35). With the bare fermion propagator $G^0(i\omega) = 1/i\omega$ they read

$$\Pi(i\nu) = -\frac{1}{2\beta} \sum_{i\omega} G(i\omega + i\nu) \frac{1}{i\omega} \quad (60a)$$

$$\chi(\mathbf{q}, i\nu) = \frac{\Pi(i\nu)}{1 + J(\mathbf{q})\Pi(i\nu)} \quad (60b)$$

$$D(i\nu) = \frac{1}{N_L} \sum_{\mathbf{q}} J^2(\mathbf{q}) \chi(\mathbf{q}, i\nu) \quad (60c)$$

$$\Sigma(i\omega) = \frac{3}{4\beta} \sum_{i\nu} D(i\nu) \frac{1}{i\omega + i\nu} \quad (60d)$$

$$G(i\omega) = [i\omega - \Sigma(i\omega)]^{-1} \quad (60e)$$

Again we first consider the static approximation, i.e., let $D(i\nu) = D(0)\delta_{\nu,0}$ in the self energy Eq.(60d). This leads

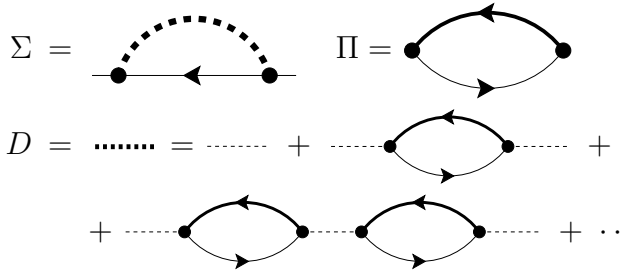


FIG. 7: The minimal self-consistent approximation (MSCA) for the disordered phase at $T > 0$ discussed in Sect. V, Eqs.(60). The full line denotes the fermion propagator Eq.(60e), which contains the self energy Σ , Eq.(60d). The thick dashed line is the renormalized interaction D , Eq.(60c). Note that in contrast to the fully self-consistent approximation shown in Fig. 2, the fermion propagator in the self energy Σ as well as one of the fermion lines in the irreducible bubble Π , Eq.(60a), remain unrenormalized (bare). These are given by $G^0(i\omega) = 1/i\omega$. In the MSCA the only self-consistent quantity is the susceptibility χ , Eq.(60b), that enters D .

to $\Sigma(i\omega) = (\bar{\omega}_s)^2 / i\omega$ and thus

$$G(i\omega) = \frac{1}{2} \left[\frac{1}{i\omega - \bar{\omega}_s} + \frac{1}{i\omega + \bar{\omega}_s} \right] \quad (61)$$

$$\bar{\omega}_s = \frac{\omega_f}{2} = \sqrt{\frac{3}{4\beta} D(0)}$$

That is, the fermion spectrum consists of two δ -peaks at $\pm \bar{\omega}_s \sim J$, which is much more close to the anticipated (pseudo) gap than the continuous one Eq.(44). Within the static approximation the gap comes out as a hard gap of $2\bar{\omega}_s$, it almost resembles the mean-field result for the ordered state at $T = 0$ given by Eq.(17). From Eq.(60a) we get

$$\Pi(i\nu) = \frac{1}{4} \frac{\bar{\omega}_s}{\bar{\omega}_s^2 - (i\nu)^2}$$

Here also the similarity to the mean-field expression Eq.(20a) is apparent. At the real axis $i\nu \rightarrow \omega + i0_+$, we find using $J(\mathbf{q}) \simeq -2dJ + Jk^2$, $\mathbf{k} = \mathbf{q} - \mathbf{Q}$,

$$\chi(\mathbf{q}, \omega) = \frac{c^2}{J} [c^2(\xi^{-2} + k^2) - \omega^2 - i\omega 0_+]^{-1} \quad (62)$$

with $c^2 = J\bar{\omega}_s^2 \Pi(0)$ and ξ^{-2} from Eq.(39). Omitting terms of $\mathcal{O}(e^{-\beta\bar{\omega}_s})$ and $\mathcal{O}(\xi^{-2})$, for $d = 2$ it is $\Pi(0) = 1/4J$ from Eq.(39), $\Pi(0) = 1/4\bar{\omega}_s$, and thus $\bar{\omega}_s = J$. The latter has to be equal to $\bar{\omega}_s = \omega_f/2$, with ω_f already derived in Eq.(41). The solution of the resulting self-consistency equation gives a correlation length and spin-wave velocity

$$\xi(T) \propto \exp(a_s J/T) , \quad a_s = \frac{\pi}{6} \simeq 0.52 , \quad c = \frac{J}{2} \quad (63)$$

That is, within the static approximation the MSCA delivers sharp ‘spin-waves’. Their dispersion $\Omega(\mathbf{q}) =$

$\sqrt{\Delta^2 + c^2 k^2} \geq \Delta$ has a gap $\Delta = c\xi^{-1}$, since at $T > 0$ the spin-rotation symmetry is not broken. In the static approximation the dynamical scaling property (3), (4) is almost trivially fulfilled by Eq.(62), since the linear term $\sim i\omega$ does not contribute: From $\chi(\mathbf{q}, \omega) = \frac{1}{J} [1 + (k\xi)^2 - (\omega/\Delta)^2 - i\omega 0_+]^{-1}$ the structure factor (51) immediately takes the form (3), with the scales ξ and $\omega_0 = \Delta$. The dynamical exponent comes out correctly as $z = 1$. The infinite lifetime of spin waves originates from the hard gap $2\bar{\omega}_s = 2J$ in the fermion propagator (61). If the static approximation in Σ is relaxed, this gap will be partly filled, and spin excitations acquire a finite damping. In that case both terms $\sim i\omega$ and $\sim \omega^2$ contribute in $\chi(\mathbf{q}, \omega)^{-1}$, and dynamical scaling becomes a non-trivial property.

A. Relation to Earlier Work

Our minimal self-consistent approximation bears similarity to a scheme that has been introduced early on in Refs. 36,37,67 and later used in Refs. 38,68 to study pseudo-gap effects caused by strong (resonant) Cooper-pair-amplitude fluctuations in low-dimensional systems. The physics is similar, except for the type of long-range fluctuations responsible for the formation of a pseudo gap. The fermion self-energy used in, e.g., Ref. 38 consists of particle-particle ladders (pair susceptibility) convoluted with a bare fermion propagator, whereas in Fig. 7 it is the particle-hole channel (magnetic susceptibility). In both cases the ladder element (or bubble) is formed with one bare and one renormalized Green’s function. Apparently, in order to obtain a pseudo-gap in the fermion spectrum due to strong collective fluctuations, an approximation with ‘reduced self consistency’ is desirable. This has also been observed in Ref. 35 for the Hubbard model in 2D close to the antiferromagnetic transition.

Supposedly, the MSCA cannot be obtained from the stationary point of an approximate free-energy functional (Φ -derivable approximation^{64,65}), since both bare and renormalized Green’s functions enter the self energy⁶⁹. However, exact equations of motion in combination with the use of cumulants (connected Green’s functions) provide an alternative way of generating self-consistent approximations in a systematic fashion. The basic approximation is to ignore the effective interaction (vertex function) of 3 and more fermions. That technique has been introduced in Ref. 67 and applied to superconductors in Refs. 36,37. In Appendix D we re-derive the MSCA for the Heisenberg model from the equations of motion.

B. Numerical Results

In the following we solve Eqs.(60) numerically, taking the frequency dependence of $D(i\nu)$ into account. Eqs.(60) are analytically continued to the real axis, $i\nu \rightarrow$

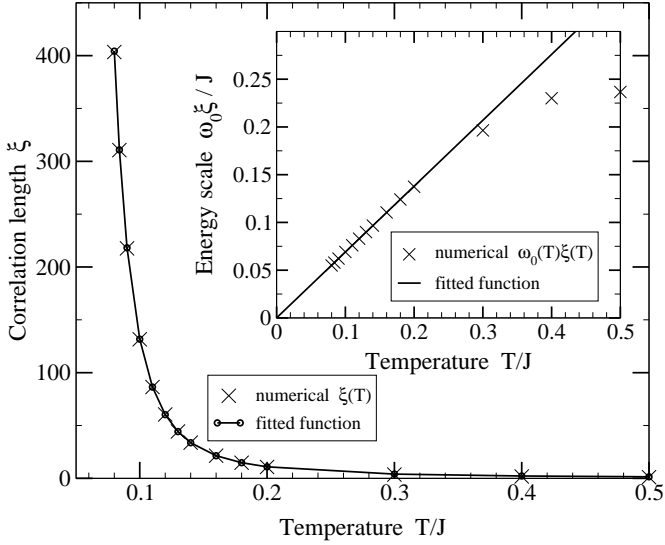


FIG. 8: **Main figure:** Correlation length $\xi(T)$ of the minimal self-consistent approximation (MSCA). Shown is the data from the numerical solution of Eqs.(60) and the function $\xi(T) = 0.362 \frac{J}{T} \exp(0.359 J/T)$ resulting from a linear regression of the data, plotted as $[t(\ln(\xi) + \ln(t))]$, to the function $[a + t \ln(b)]$, $t = T/J$ for $T \leq 0.18 J$. **Inset:** Energy scale $\omega_0(T)$ of the MSCA, extracted from the numerical solution of Eqs.(60) using Eq.(54). Shown is the numerical data for $\omega_0(T)\xi(T)$ and the function $\omega_0\xi = 0.690 T$, obtained from a linear regression for $T \leq 0.18 J$. The extrapolation to $T = 0$ is $\omega_0(0)\xi(0) = 0.00003 J$.

$\omega + i0_+$, leading to Eqs.(A2). These are solved by numerical iteration. Numerically stable solutions have been obtained for temperatures $T \gtrsim 0.08 J$, corresponding to correlation lengths $\xi \lesssim 400$ lattice spacings. Correlation length $\xi(T)$ and energy scale $\omega_0(T)$ are extracted from the numerical data using Eq.(39) and Eq.(54), respectively. For $T \lesssim 0.2 J$, where $\xi \gtrsim 10$, these are well fitted by

$$\xi(T) \propto \frac{J}{T} \exp(a J/T) , \quad a = 0.36 , \quad \omega_0(T) \propto \frac{T}{\xi} \quad (64)$$

Fig. 8 shows the numerical data and the fits.

The result for ξ contains a factor $1/T$ in front of the usual exponential. In that respect ξ is different from the static approximation discussed above. The $1/T$ prefactor has been obtained for the QNL σ M, as long as the RG calculation is restricted to 1-loop order¹⁰. The energy scale $\omega_0 \sim \xi^{-1}$, which we confirm by analytical calculation below, is now consistent with a dynamical exponent $z = 1$. The MSCA also features short-range order in the dynamical structure factor $S(\mathbf{q}, \omega)$: The scaling function $\Phi(k\xi, \omega/\omega_0)$, extracted from the numerical data using Eq.(55), is plotted in Fig. 9. Apparently the single peak at $\omega = 0$ splits into two peaks located symmetrically to $\omega = 0$, if the inverse wave vector is smaller than the correlation length, $k\xi > 1$. (Negative energies are not shown in the figure). These peaks move away from $\omega = 0$ with increasing k , similar to damped spin waves. According

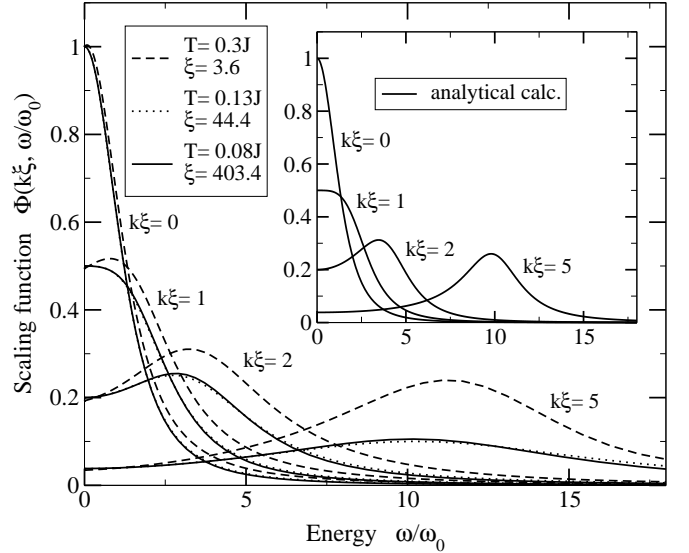


FIG. 9: **Main figure:** Dynamical structure factor from the numerical solution of the MSCA, Eqs.(60), at low energies $\sim \omega_0$. Plotted is the scaling function $\Phi(k\xi, \omega/\omega_0)$ as defined in Eq.(55). Φ is shown for fixed wave vectors $k = 0, \xi^{-1}, 2\xi^{-1}, 5\xi^{-1}$, each for 3 different temperatures corresponding to $\xi = 3.6, 44.4, 403.4$. The curves for $\xi = 44.4, 403.4$ are almost indistinguishable. For wave vectors $k > \xi^{-1}$ a propagating ‘spin-wave’ mode becomes visible. **Inset:** The scaling function $\Phi(k\xi, \omega/\omega_0)$ of the analytical calculation described in Sect. V C, Eq.(85), for $p = 0.25$.

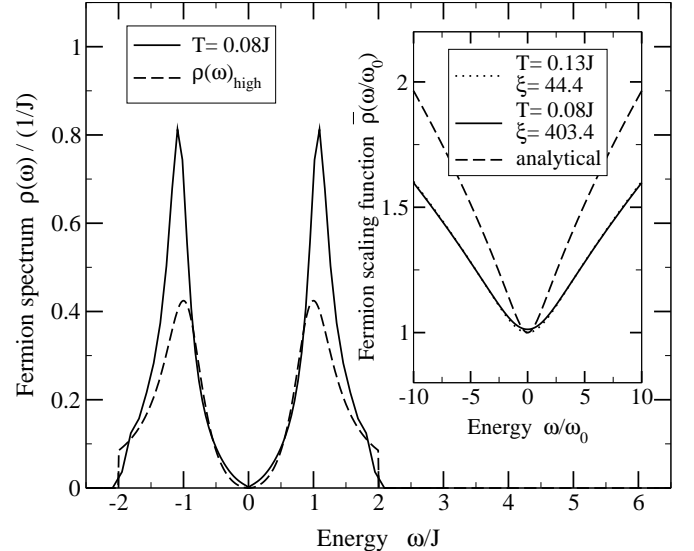


FIG. 10: **Main figure:** Numerical spectral function $\rho(\omega)$ of the fermion (full line) in the MSCA, Eqs.(60), in the high-energy range $\sim J$. The dashed line is the high-energy approximation Eq.(77) from the analytical calculation. **Inset:** Numerical $\rho(\omega)$ at low energies $\sim \omega_0$, shown is the scaling function $\bar{\rho}(\omega/\omega_0) = \frac{3JT}{\omega_0} \rho(\omega)$ introduced in Eq.(74). The curves for $\xi = 44.4$ and 403.4 (dotted and full line, respectively) are almost identical. The dashed line is $\bar{\rho}(\omega/\omega_0)$ from the analytical calculation, Eq.(74).

to the analytical calculation, their dispersion $\bar{\omega}(k\xi)$ becomes linear for $k\xi \gg 1$, $|\bar{\omega}|/\omega_0 = 2k\xi$. The numerical data obeys scaling for temperatures below $\sim 0.1J$, corresponding to $\xi > 10$. Dynamical scaling is also visible in the spectrum $\rho(\omega)$ of the fermions. The inset of Fig. 10 shows the scaling function $\bar{\rho}(\omega/\omega_0) = \frac{3JT}{\omega_0} \rho(\omega) \propto \xi \rho(\omega)$ at low energies $\sim \omega_0$. The curves for $\xi \simeq 40$ (dotted line) and for $\xi \simeq 400$ (full line) lie on top of each other. The definition of $\bar{\rho}$ is a result of the analytical calculation to be presented below, Eq.(74). The main Figure 10 shows an overall view of $\rho(\omega)$, the anticipated pseudo-gap structure is apparent, with two broad peaks near $\pm J$.

C. Analytical Calculation: Origin of Scaling and the Propagating Mode

In order to confirm the numerical result for the energy scale, $\omega_0 \propto T/\xi$, and to obtain some insight into the origin of the dynamical scaling numerically observed at low energies, we finally discuss an approximate analytical solution of Eqs.(60) for $T \ll J$ and $\xi \gg 1$, which does not make use of the static approximation.

We start from the following set of equations, which is derived in Appendix C from Eqs.(60),

$$\chi(\mathbf{q}, \omega) = \frac{\xi^2}{J} \frac{1}{1 + (\xi k)^2 - R(\omega)} \quad (65a)$$

$$R(\omega) = 16J\xi^2 \tilde{\Pi}(\omega) \quad (65b)$$

$$\begin{aligned} \tilde{\Pi}(\omega) &= i \frac{\pi}{4} \tanh(\omega/2T) \rho(\omega) + \\ &+ \frac{\omega^2}{2} \int_0^\infty d\varepsilon \rho(\varepsilon) \frac{\tanh(\varepsilon/2T)}{\varepsilon(\varepsilon^2 - \omega^2)} \end{aligned} \quad (65c)$$

$$\rho(\omega) = -\frac{1}{\pi} \text{Im}[\omega - \Sigma(\omega)]^{-1} \quad (65d)$$

$$\Sigma(\omega) = \frac{3}{8\pi} \int_{-\infty}^\infty d\varepsilon \text{Im}D(\varepsilon) \frac{\coth(\varepsilon/2T)}{\omega - \varepsilon + i0_+} \quad (65e)$$

$$D(\omega) = \frac{4J}{\pi} \int_0^{(k_c\xi)^2} dx \frac{1}{1 + x - R(\omega)} \quad (65f)$$

The correlation length ξ is given by Eq.(39) as before, k_c denotes a wave-vector cut off of $\mathcal{O}(1)$. The static $\omega = 0$ value of Π required for Eq.(39) reads

$$\Pi(0) = \frac{1}{2} \int_0^\infty d\varepsilon \tanh(\varepsilon/2T) \frac{\rho(\varepsilon)}{\varepsilon} \quad (65g)$$

In Eq.(65a) the static properties of χ have been separated from its dynamics, which are determined by $\Pi(0)$ (through ξ) and $\tilde{\Pi}(\omega)$ (through $R(\omega)$), respectively. See Appendix C for details.

For the dynamical part $R(\omega)$ we consider the ansatz

$$R(\omega) = i\omega/\omega_0 + p(\omega/\omega_0)^2 \quad (66)$$

ω_0 and p are independent of ω . This form of $R(\omega)$, inserted in Eq.(65a), is able to describe the relaxation

regime $k\xi \lesssim 1$ as well as propagating ‘spin-wave’ modes for $k\xi \gtrsim 1$.

With Eq.(66) the imaginary part of the renormalized interaction (65f) becomes

$$\text{Im}D(\omega) = \frac{4J}{\pi} \arctan(\omega/\omega_0) \Theta(\omega_C - |\omega|) \quad (67)$$

$\text{Im}D(\omega)$ is essentially the local spectral function for spin excitations. In Eq.(67) all features of $\text{Im}D(\omega)$ for $\omega > \omega_0$ have been replaced by a constant; $\omega_C \sim 2J$ is a high-energy cut-off.

The energy scale ω_0 is exponentially small, $\omega_0 \sim J/\xi$. This already follows from the real part at $\omega = 0$, which results from Eq.(65f) as $\text{Re}D(0) = \frac{8J}{\pi} \ln(k_c\xi)$ and should roughly compare to the result of a Kramers–Kronig transformation applied to Eq.(67), $\text{Re}D(0) \simeq \frac{2J}{\pi} \ln(\omega_C/\omega_0)$.

In order to calculate ω_0 and p with Eq.(67) as input, Eq.(65c) is expanded up to $\mathcal{O}(\omega^2)$ and the parameters are identified as

$$\frac{1}{\omega_0} = \frac{2\pi J}{T} \xi^2 \rho(0) \quad (68)$$

$$p = 8J\omega_0^2 \xi^2 \int_0^\infty d\varepsilon \left. \frac{\tanh(\varepsilon/2T) \rho(\varepsilon)}{\varepsilon(\varepsilon^2 - \omega^2)} \right|_{\omega \rightarrow 0} \quad (69)$$

The energy scale ω_0 is extracted easily with the observation that the self energy at $\omega = 0$ is imaginary, $\text{Re}\Sigma(0) = 0$. This comes from the particle–hole symmetry of the Hamiltonian (8) at 1/2-filling, $\mu^f = 0$. With Eqs.(65e) and (67) we get $\text{Im}\Sigma(0) = -3JT/\pi\omega_0$, leading to $\rho(0) = -(\pi\text{Im}\Sigma(0))^{-1} = \omega_0/3JT$. With Eq.(68) a self-consistency condition for ω_0 follows, with the solution

$$\omega_0 = \sqrt{\frac{3}{2\pi}} \frac{T}{\xi} , \quad \rho(0) = \frac{1}{J} \sqrt{\frac{1}{6\pi}} \frac{1}{\xi} \quad (70)$$

Apparently the dynamical exponent is $z = 1$.

The calculation of the parameter p requires an integration over the fermion spectrum $\rho(\varepsilon)$. Therefore we approximate $\Sigma(\omega)$ for low $\omega \lesssim \omega_0 \ll T$ and high energies $\omega \gg \omega_0$ separately, at low temperature $T \ll J, \omega_C$. For $\omega \lesssim \omega_0$ we have from Eq.(65e) and (67),

$$\text{Im}\Sigma(\omega)_{low} = -\frac{3JT}{\pi} \frac{\arctan(\omega/\omega_0)}{\omega} \quad (71)$$

The real part is obtained from the Kramers–Kronig transform

$$\text{Re}\Sigma(\omega) = \frac{1}{\pi} \int_{-\infty}^\infty d\varepsilon \frac{\text{Im}\Sigma(\varepsilon)}{\varepsilon - \omega} \quad (72)$$

as

$$\begin{aligned} \text{Re}\Sigma(\omega)_{low} &= \frac{6JT}{\pi^2} \omega \int_0^\infty d\varepsilon \frac{\arctan(\varepsilon/\omega_0)}{\varepsilon(\varepsilon^2 - \omega^2)} \\ &= \frac{3JT}{2\pi} \frac{\ln[1 + (\omega/\omega_0)^2]}{\omega} \end{aligned} \quad (73)$$

Since $\omega \sim \omega_0$ the self-energy is large, $|\Sigma(\omega)|_{low} \sim JT/\omega_0 \propto J\xi \gg \omega$, and the spectrum (65d) is given by $\rho(\omega)_{low} = \frac{1}{\pi} \text{Im}[1/\Sigma(\omega)] + \mathcal{O}(\xi^{-2})$. Accordingly the fermion spectrum at low energy takes the form

$$\begin{aligned} \rho(\omega)_{low} &= \frac{\omega_0}{3JT} \text{Im} \frac{y}{\frac{1}{2} \ln(1+y^2) - i \arctan(y)} \\ &\equiv \frac{\omega_0}{3JT} \bar{\rho}(y) \quad , \quad y = \omega/\omega_0 \end{aligned} \quad (74)$$

where some scaling function $\bar{\rho}(y)$ has been identified. For $y \rightarrow 0$ the previous result (70) for $\rho(0)$ is recovered. As anticipated earlier, $\rho(\omega)$ shows an incomplete gap, the spectral weight in the region $\omega \lesssim \omega_0$ is $\sim 1/J\xi$. The scaling function $\bar{\rho}(\omega/\omega_0)$ is plotted in the inset of Fig. 10, it qualitatively agrees with the result from the numerical solution.

In the regime of high energy $\omega \gg \omega_0$ the imaginary part of Σ reads

$$\text{Im}\Sigma(\omega)_{hi} = -\frac{3J}{4} \coth(|\omega|/2T) \Theta(\omega_C - |\omega|) \quad (75)$$

and the real part is calculated using Eq.(72),

$$\begin{aligned} \text{Re}\Sigma(\omega)_{hi} &= \frac{3J}{2\pi} \omega \int_{\omega_0}^{\omega_C} d\varepsilon \frac{\coth(\varepsilon/2T)}{\omega^2 - \varepsilon^2} \\ &\simeq \frac{3J}{2\pi} \omega \left[\int_{\omega_0}^T d\varepsilon \frac{2T}{\varepsilon(\omega^2 - \varepsilon^2)} + \int_T^{\omega_C} d\varepsilon \frac{1}{\omega^2 - \varepsilon^2} \right] \end{aligned}$$

A lower integral boundary ω_0 has been introduced, since in Eq.(65e) the arctan from Eq.(67) cuts off the $1/\varepsilon$ divergence coming from the $\coth(\varepsilon/2T)$. In the resulting $\text{Re}\Sigma_{hi}$ we keep only the terms $\sim 1/\omega$ showing the strongest ω dependence, that is,

$$\text{Re}\Sigma(\omega)_{hi} = \frac{\bar{\omega}^2}{\omega} \quad , \quad \bar{\omega}^2 = \frac{3JT}{\pi} \ln(T/\omega_0) \quad (76)$$

Thus we arrive at the fermion spectrum in the high-energy regime,

$$\rho(\omega)_{hi} = \frac{1}{\pi} \text{Im} \frac{\Theta(\omega_C - |\omega|)}{\bar{\omega}^2/\omega - \omega - iJ\frac{3}{4} \coth(|\omega|/2T)} \quad (77)$$

This spectrum has two peaks at $\omega = \pm \bar{\omega}$, similar to the result from the static approximation appearing below Eq.(60), $\bar{\omega}$ and $\bar{\omega}_s$ are of the same order of magnitude $\sim J$. However, here the peaks are no longer δ -like but show a significant width. $\rho(\omega)_{hi}$ is plotted and compared to the numerical solution in Fig. 10.

With Eqs.(74) and (77) the parameter p can now be estimated: The integral in Eq.(69) is split into three regions and the $\tanh(\varepsilon/2T)$ approximated,

$$\begin{aligned} p &= \frac{12}{\pi} JT^2 \left[\frac{1}{2T} \int_0^{\alpha\omega_0} d\varepsilon \frac{\rho(\varepsilon)_{low}}{\varepsilon^2 - \omega^2} \Big|_{\omega \rightarrow 0} \right. \\ &\quad \left. + \frac{1}{2T} \int_{\alpha\omega_0}^T d\varepsilon \frac{\rho(\varepsilon)_{hi}}{\varepsilon^2} + \int_T^{\omega_C} d\varepsilon \frac{\rho(\varepsilon)_{hi}}{\varepsilon^3} \right] \\ &\equiv \frac{12}{\pi} JT^2 [I_{\omega_0} + I_T + I_J] \end{aligned} \quad (78)$$

The result (70) for ω_0 has been inserted. α is a number, $\alpha\omega_0$ indicates where ρ_{low} and ρ_{hi} roughly match. We assume that α can be chosen constant at small T , where $\omega_0 \ll \alpha\omega_0 \ll T \ll J, \omega_C$. We seek the leading T -dependence of p .

With Eq.(74) the low-energy contribution becomes $I_{\omega_0} = \lim_{y \rightarrow 0} \frac{1}{6JT^2} \int_0^\alpha dx \bar{\rho}(x)/(x^2 - y^2)$, that is,

$$I_{\omega_0} \propto 1/JT^2 \quad (79)$$

For estimating I_T the spectrum (77) is expanded for $|\omega| \leq T \ll J, \bar{\omega}$, i.e.,

$$\begin{aligned} \rho(\omega)_{hi} &= \frac{1}{\pi} \text{Im} \left[\frac{\omega}{\bar{\omega}^2} \left\{ 1 + i \frac{3J}{2\bar{\omega}} \frac{T}{\bar{\omega}} \text{sign}(\omega) + \mathcal{O}\left(\frac{\omega^2, T^2}{\bar{\omega}^2}\right) \right\} \right] \\ &= \frac{3JT}{2\pi\bar{\omega}^4} |\omega| \end{aligned} \quad (80)$$

and we arrive at

$$I_T = \frac{3J}{4\pi\bar{\omega}^4} \left[\ln\left(\frac{T}{\omega_0}\right) - \ln(\alpha) \right] = \frac{1}{4T\bar{\omega}^2} \left[1 + \mathcal{O}\left(\frac{T}{J}\right) \right]$$

The leading T -dependence of $\bar{\omega}$ is a constant, $\bar{\omega} \sim J$ (see below), and we find

$$I_T \propto 1/J^2 T \quad (81)$$

In the high-energy contribution I_J we use Eq.(77) with $\coth(|\omega|/2T) \simeq 1$. The dominant contribution to the integral in I_J comes from the lower bound T . That is, ρ_{hi} may be expanded as above omitting terms $\mathcal{O}(\omega/J)$, which results in $\rho(\omega)_{hi} = (3J/4\bar{\omega}^4) \omega^2$. With $\bar{\omega} = \text{const.} \sim J$ its contribution to p is

$$I_J \propto \ln(J/T)/J^3 \quad (82)$$

Collecting Eqs.(79), (81), (82) together, the leading contribution to p for $T \rightarrow 0$ is the lowest-energy part I_{ω_0} . Its T -dependence cancels the T^2 prefactor in Eq.(78), and

$$p \propto JT^2 I_{\omega_0} = \text{const.} \quad (83)$$

Thus, in leading order T/J the parameter p comes out as a (dimensionless) finite constant. With p in Eq.(66) being constant, the dynamical susceptibility (65a) immediately assumes a scaling form, $\chi(\mathbf{q}, \omega) = \frac{\xi^2}{J} [1 + x^2 - py^2 - iy]^{-1}$ with length and energy scales ξ and ω_0 in $x = k\xi$, $y = \omega/\omega_0$ given by

$$\omega_0 \propto T/\xi \quad , \quad \xi \propto \exp(0.63 J/T) \quad (84)$$

The former has been given in Eq.(70), the latter will be derived below.

The structure factor defined in Eq.(51) then takes the scaling form stated in Eqs.(3), (4), with the scaling functions

$$\varphi(x) = \frac{1}{1+x^2} \quad , \quad \Phi(x, y) = \frac{1+x^2}{(1+x^2 - py^2)^2 + y^2} \quad (85)$$

The precise value of p is not known from the above calculation. The ‘shape function’ $\Phi(x, y)$ is plotted in the inset of Fig. 9 for $p = 1/4$. It consists of a single peak at $\omega = 0$ for wave vectors in the relaxation regime $x = k\xi \ll 1$, which splits into two peaks located symmetrically to $\omega = 0$ for $x = k\xi > \bar{x}$ in the regime of propagating modes. The boundary between these regimes is given by $\partial_y^2 \Phi(\bar{x}, y)|_{y=0} = 0$ and reads $\bar{x} = \sqrt{(1-2p)/2p}$. The scaling function Φ compares well to the numerical result shown in the main Figure 9. Apparently the choice $p = 1/4$ corresponding to $\bar{x} = 1$ is consistent with the numerics. For energies $\omega > \omega_0$ the damping (i.e., the width of the peaks for $k\xi > 1$) comes out larger in the numerical calculation, supposedly due to higher-order terms omitted in the ansatz (66) for $R(\omega)$ in Eq.(65a). The ‘spin-wave’ dispersion $\bar{y}(x) = \bar{\omega}(x)/\omega_0$ of the peak-maximum is determined from $\partial_y \Phi(x, \bar{y}) = 0$. At large wave vectors $k\xi \gg \bar{x}$ it becomes linear, $\bar{\omega}/\omega_0 \simeq k\xi/\sqrt{p}$.

Finally the correlation length already given in (84) has to be derived self-consistently from Eq.(65g) and (39). The integral in Eq.(65g) is split into three parts, with the $\tanh(\varepsilon/2T)$ approximated appropriately,

$$\begin{aligned} \Pi(0) &= \frac{1}{4T} \int_0^{\alpha\omega_0} d\varepsilon \rho_{low}(\varepsilon) + \frac{1}{4T} \int_{\alpha\omega_0}^T d\varepsilon \rho_{hi}(\varepsilon) + \\ &\quad + \frac{1}{2} \int_T^{\omega_C} d\varepsilon \frac{\rho_{hi}(\varepsilon)}{\varepsilon} \\ &\equiv \Pi(0)_{\omega_0} + \Pi(0)_T + \Pi(0)_J \end{aligned}$$

With ρ_{low} from Eq.(74) inserted, the low-energy part becomes $\Pi(0)_{\omega_0} = \frac{\omega_0^2}{12JT^2} \int_0^\alpha dy \hat{\rho}(y) \propto (\omega_0/T)^2/J \propto 1/(\xi^2 J)$. Its contribution to the self-consistency condition (39) can be ignored, since $\Pi(0) = 1/4J + \mathcal{O}(\xi^{-2})$. In $\Pi(0)_T$ we can again use Eq.(80), i.e., $\rho_{hi}(\varepsilon) = \frac{3JT}{2\pi\bar{\omega}^4} |\varepsilon|$, leading to $\Pi(0)_T \propto JT^2/\bar{\omega}^4 \sim T^2/J^3$, which also can be ignored at small $T \ll J$. The dominant contribution to $\Pi(0)$ comes from high energies: Using ρ_{hi} , Eq.(77), with $\omega > T$ results in

$$\begin{aligned} \Pi(0)_J &= \frac{1}{2\pi} \int_T^{\omega_C} \frac{d\varepsilon}{\varepsilon} \text{Im} \frac{1}{\bar{\omega}^2/\varepsilon - \varepsilon - i\frac{3}{4}J} \\ &= \frac{2}{3\pi J} \int_{4T/3J}^{4\omega_C/3J} du \frac{u}{(g^2 - u^2)^2 + u^2} \end{aligned}$$

with $g^2 = (4\bar{\omega}/3J)^2 = \frac{16}{3\pi} \frac{T}{J} \ln(T/\omega_0)$. The above expression has to fulfill $\Pi(0)_J = \Pi(0) = 1/4J$, giving an implicit equation for g^2 and therefore $\xi \propto T/\omega_0$. The exponential part of ξ can be extracted with $T \rightarrow 0$ and $\omega_C \rightarrow \infty$ in the integral boundaries. We find $g^2 = 1.07$ and with Eq.(70) the correlation length is $\xi(T) = \sqrt{\frac{3}{2\pi}} \exp(aJ/T)$, $a = 3\pi g^2/16 = 0.63$.

VI. QUALITY OF THE CONSTRAINT

The representation of spin operators in auxiliary particles, Eq.(5), is valid only if the Fock space of canon-

ical fermions is restricted to the subspace with $Q_i = \sum_\alpha f_{i\alpha}^\dagger f_{i\alpha} = 1$ on each lattice site i . We have argued in Sects. II, III, IV that the local charge density Q_i is a conserved quantity in the approximations considered in this paper, $\partial_\tau Q_i(\tau) = 0$. In particular there is no spontaneous breaking of the corresponding gauge symmetry in the 1/2-filled Heisenberg model. However, we have replaced the local constraint $Q_i = 1$ by a global one, $\langle Q_i \rangle = 1 \Leftrightarrow Q_{tot} = \sum_1^{N_L} Q_i = N_L$, since in that case we were able to use standard many-body techniques.

The true ground state of the model Hamiltonian belongs to the physical sector of the Hilbert space and thus features a total charge $Q_{tot} = N_L$ with a homogeneous density $Q_i = 1$. With just the global constraint $Q_{tot} = N_L$ in effect, this ground state might be (almost) degenerate with multiplets of unphysical states where Q_{tot} is distributed inhomogeneously on the lattice. In that case the unphysical states mix spectral weight into correlation functions like the spin susceptibility. However, one can hope that the separation in energy of these unphysical states from the ground state is finite, and at $T \rightarrow 0$ the correlation functions actually measure physical processes. Since the Q_i are conserved, the excited states generated in the correlation function (e.g., through a spin flip) remain in the physical sector.

The gap of the lowest unphysical state to the ground state will depend on the physics of the latter. For the AF ordered state of the mean-field theory (see Sect. III) chances are good: The Néel state $|AF\rangle = |AF; \{Q_i = 1\}\rangle$ is compared to some state $|AF'\rangle = |AF; Q_l = 0, Q_{l'} = 2, \{Q_i = 1, i \neq l, l'\}\rangle$, where a fermion has been transferred from some site l to another site l' . Thus the spins on sites l and l' have disappeared, and the unphysical state $|AF'\rangle$ is higher in energy by $2J$, equivalent to 8 lost J -bonds. The gap $2J$ is just the charge-transfer gap $\lim_{T \rightarrow 0} 2|m_A| = 2J$ in the spectrum Eq.(17) of the auxiliary fermions.

The above reasoning can easily be verified by calculation, at least for the mean-field theory. The local charge (constraint) fluctuations on an arbitrary site i are

$$\begin{aligned} \langle(\Delta Q_i)^2\rangle &= \langle Q_i Q_i \rangle - \langle Q_i \rangle \langle Q_i \rangle \\ &= -\frac{1}{\beta} \sum_{i\nu} \frac{1}{\beta} \sum_{i\omega} \text{Tr}[\overline{G}_i(i\omega + i\nu) \overline{G}_i(i\omega)] \end{aligned}$$

involving a charge-response bubble built similar to the spin response Eq.(19)⁷⁰. With the fermion Green’s function in mean field, Eq.(15), this becomes

$$\langle(\Delta Q_i)^2\rangle = 2f(m_A)[1 - f(m_A)] \quad (86)$$

for $i \in A$ or B sublattice. Above the mean-field transition temperature, $T > T_N = J/2$, we have $m_A = 0$ and therefore $\langle(\Delta Q_i)^2\rangle = 1/2$. That is, the constraint is significantly violated. However, in the AF ordered phase $T < T_N$ we have $|m_A| > 0$ and charge fluctuations are suppressed; at $T \ll T_N$ Eq.(86) leads to activated behavior, $\langle(\Delta Q_i)^2\rangle = 2 \exp(-2J/T)$, revealing the above-mentioned gap $2J$ between the Néel ground state $|AF\rangle$

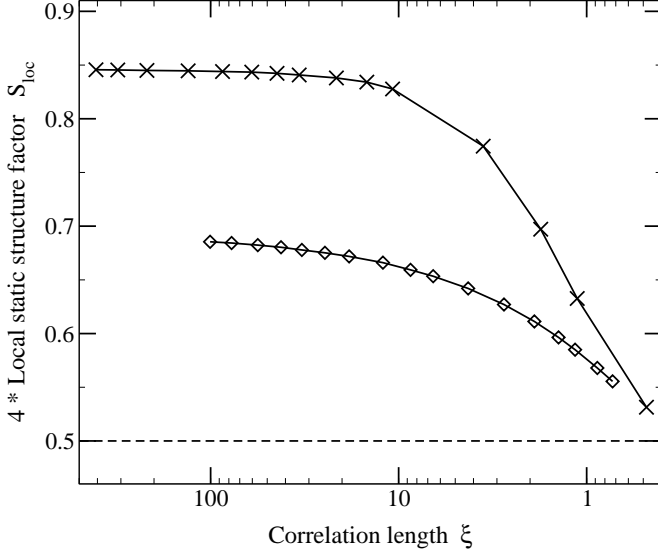


FIG. 11: Influence of constraint fluctuations on the local spin moment $S_{loc}^{st} = \langle (S_i^x)^2 \rangle$, calculated numerically using Eq.(B1). Shown is $4S_{loc}^{st}$ as function of the correlation length $\xi(T)$ for the MSCA (crosses) and the fully self-consistent approximation (diamonds). For $\xi > 10$ the MSCA reaches 85% of the exact value $4S_{loc}^{st} = \frac{4}{3}S(S+1) = 1$. The dashed line indicates the high- T limit $1/2$.

and the lowest unphysical one $|AF'\rangle$. At $T = 0$ the constraint is exactly fulfilled.

For the minimal self-consistent approximation we do not have an expression for the free energy⁶⁹ and thus do not know how to calculate $\langle (\Delta Q_i)^2 \rangle$ consistently. An alternative test for the constraint is the local spin moment, which reads in the paramagnetic phase $\langle S_i^\mu \rangle = 0$,

$$\langle (\mathbf{S}_i)^2 \rangle = \sum_\mu \langle S_i^\mu S_i^\mu \rangle = 3S_{loc}^{st}, \quad S_{loc}^{st} = \langle S_i^x S_i^x \rangle$$

Since our system of interacting auxiliary fermions represents a pure spin-1/2 model, we have $\langle (\mathbf{S}_i)^2 \rangle = S(S+1) = 3/4$, and the local static structure factor should be $S_{loc}^{st} = 1/4$. Fluctuations of the fermion occupancy Q_i will reduce S_{loc}^{st} from this exact value. At high temperature $T \gg J$ the susceptibility Eq.(18) is given by the simple fermion bubble Eq.(19), i.e.,

$$S_{loc}^{st} = \frac{1}{\beta} \sum_{i\nu} \Pi_i^{xx}(i\nu) = \frac{1}{2} \langle f_{i\uparrow}^\dagger f_{i\uparrow} \rangle \langle f_{i\downarrow} f_{i\downarrow}^\dagger \rangle = \frac{1}{8} \quad (87)$$

where Eq.(10) and $\langle f_{i\uparrow}^\dagger f_{i\uparrow} \rangle = \langle f_{i\downarrow}^\dagger f_{i\downarrow} \rangle = \langle Q_i \rangle / 2 = 1/2$ has been used. That is, constraint fluctuations reduce the spin moment to 50% of its physical value. Note that this holds for any density of states of the fermions, including the case of free spins ($J = 0$). When temperature is lowered below $\simeq J$ in the interacting system, we expect the spin moment to be restored as a consequence of a strong reduction of $\langle (\Delta Q_i)^2 \rangle$ in the short-range ordered regions. S_{loc}^{st} has been calculated numerically using

Eq.(B1), the result for the MSCA is shown in Fig. 11 as crosses. In fact the spin moment saturates to $\simeq 0.85$. The fully self-consistent approximation, which does not show short-range order, reaches $\simeq 0.68$ (shown as diamonds in Fig. 11).

For comparison we also discuss the spin moment in mean-field theory: At high $T \gg T_N$ Eq.(87) holds, and we have a reduced moment as above, $\langle (\mathbf{S}_i)^2 \rangle = 3\frac{1}{8}$. At $T \ll T_N$, in the presence of long-range AF order, the spin moment is

$$\langle (\mathbf{S}_i)^2 \rangle = S_{loc}^{st||} + 2S_{loc}^{st\perp}, \quad S_{loc}^{st\perp} = \frac{1}{N_L} \sum_{\mathbf{q}} S^\perp(\mathbf{q})$$

In the longitudinal direction just the condensate contributes, $S_{loc}^{st||} = \langle S_A^z \rangle^2$, since fluctuations have vanishing weight, $\langle S_i^z S_i^z \rangle_{conn} \sim \exp(-J/T)$. The transversal contribution $S_{loc}^{st\perp}$ measures the spectral weight of spin waves and reads, from Eq.(28),

$$S_{loc}^{st\perp} = \frac{1}{2} |\langle S_A^z \rangle| (1 + 2\epsilon) \Rightarrow \langle (\mathbf{S}_i)^2 \rangle = \frac{1}{4} [1 + 2(1 + 2\epsilon)]$$

with $|\langle S_A^z \rangle| = 1/2 + \mathcal{O}(e^{-J/T})$ and the ϵ introduced in Eq.(33). At $T = 0$ the loop integral $\epsilon = 0.197$ is finite in 2D. The spin moment is fully restored, the contribution of (transversal) magnons is even overestimated in spin-wave theory.

VII. SUMMARY AND CONCLUSION

This paper presented a study of critical fluctuations in the quantum Heisenberg antiferromagnet in two dimensions. Our starting point is to re-write the spin-1/2 operators in (unphysical) fermionic auxiliary particles, which enables the use of standard many-body techniques based on Feynman diagrams. Although the Heisenberg and the t - J -model have frequently been studied on mean-field level, the problem of strong long-range fluctuations in the two-dimensional plane has not been considered before by this type of approach.

The ground state at zero temperature $T = 0$ shows long-range antiferromagnetic order and can be treated in mean-field theory and perturbative (in $1/S$) corrections. The auxiliary fermions form a simple spin-density-wave state, their density of states consists of two delta peaks separated by a large gap $2J$. Results for magnetization, spin-wave velocity and -weight have been derived in Sect. III. We found even quantitative agreement with conventional spin-wave theory.

At finite temperature the perturbation theory in $1/S$ breaks down, and the susceptibility has to be treated self-consistently in order to suppress the mean-field transition temperature $T_N = J/2$ down to zero, as required by the theorem of Mermin and Wagner. In Sect. IV we considered the simplest skeleton-diagram expansion in the renormalized fermion-propagator that provides

this feature. Within a static (classical) approximation (see Sect. IV A) the self-consistency problem can be solved analytically, leading to a correlation length $\xi(T) \propto \exp(aJ/T)$ and an exponentially small energy scale $\omega_0 \propto J\xi^{-z}$, in agreement with the existing theoretical and experimental work. The so-called dynamical scaling relation¹¹ is also fulfilled. However, the dynamical exponent $z = 2$ is incorrect, and the spin-excitation spectrum lacks a spin-wave like propagating mode. Such a (damped) mode should appear at larger wave vectors as a consequence of short-range order. The analytical results have been confirmed by numerical calculation in Sect. IV B.

We argued that the lack of ‘spin waves’ is due to a large density of states $\rho(\omega \simeq 0) \sim 1/J$ of the auxiliary particles at the Fermi energy $\omega = 0$, which causes an extreme overdamping. It turns out that this problem can be cured by reducing the amount of self-consistency: In the skeleton-diagram expansion both the susceptibility and the Green’s function of fermions are subject to their respective self-consistency loops, while being coupled to each other through the fermion self-energy. In the MSCA presented in Sect. V, which is not based on skeleton diagrams, the additional loop for the fermion propagator is avoided. The results obtained from the numerical iteration of this approximation are very satisfactory. In particular we find $\xi(T) \propto \frac{1}{T} \exp(0.359 J/T)$ and the energy scale $\omega_0 \sim 1/\xi$, i.e., the dynamical exponent is $z = 1$. The spin-excitation spectrum now features dynamical scaling as well as a propagating mode for wave vectors $k\xi > 1$. k denotes the offset from the Néel wave vector. The MSCA equations have also been solved by analytical calculation in Sect. V C, confirming the energy scale $\omega_0 = \sqrt{3/2\pi} T/\xi$. In the MSCA the spectral function $\rho(\omega)$ of auxiliary fermions features the anticipated strong suppression (pseudo gap) at the Fermi energy. The spectral weight at $\omega = 0$ is exponentially small, $\rho(0) \propto 1/J\xi$, and at low energies $\rho(\omega)$ shows dynamical scaling, $\rho(\omega) = \frac{\omega_0}{3J\pi} \bar{\rho}(\omega/\omega_0)$.

Our MSCA is technically and physically related to earlier work on low dimensional superconductors and the 2D Hubbard model, where long-range fluctuations of the superconducting or magnetic order-parameter amplitude cause a pseudo gap in the single-particle density of states. References have been given in Sect. V A. Supposedly there is no Φ -functional available⁶⁹ which could have served as a systematic basis for the approximation scheme. However, these schemes follow quite naturally from a sequence of equations of motion in combination with a cumulant decomposition of higher-order vertex functions. This type of method has been used in the above-mentioned studies on superconductors and is applied to the present problem in App. D.

During all calculations performed in this paper the auxiliary-particle constraint $Q_i = \sum_{\alpha} f_{i\alpha}^{\dagger} f_{i\alpha} = 1$ has been treated in a mean-field fashion, $\langle Q_i \rangle = 1$. Although it turns out that the fermions remain strictly local at 1/2-filling (no intersite hopping), on-site fluctu-

ations $\langle (\Delta Q_i)^2 \rangle$ into unphysical sectors of Hilbert space are not a priori suppressed. We did not attempt to improve on the constraint, e.g., by including a fluctuating Lagrange multiplier $\lambda_i(\tau)$ in the action Eq.(8) via the term $\int_0^{\beta} d\tau \sum_i \lambda_i(\tau) [1 - Q_i(\tau)]$. However, as has been explored in Sect. VI, the actual strength of constraint fluctuations at low temperature depends on the physics of the ground state. Measuring the local spin moment $\langle (\mathbf{S}_i)^2 \rangle$ in the MSCA revealed reasonably small fluctuations $\langle (\Delta Q_i)^2 \rangle$ at $T \ll J$. This is due to the magnetic order appearing on short length scales. At $T = 0$, with long-range order present, we even find $\langle (\Delta Q_i)^2 \rangle = 0$ in mean-field theory.

A major question remaining open is whether the theory violates spin-rotation symmetry. In Sect. IV C it has been shown that a straight-forward application of the conserving-approximation scheme in two dimensions leads to a spurious phase transition at some $\hat{T}_N \sim J$, because the susceptibility is modified by additional vertex corrections that are not part of the self-consistency loop. However, since approximations constructed from this scheme do respect conservation laws in the sense of a sufficient condition, it is worth testing our MSCA for spin-rotation symmetry ‘by hand’, e.g., through confirming the Goldstone peak at $\mathbf{q} = (\pi, \pi)$ and $\omega = 0$ in the long-range ordered state at $T = 0$. This requires a self-consistent calculation at $\langle \mathbf{S} \rangle \neq 0$, which we postpone to future work.

We think that the auxiliary-fermion approach proved quite useful for dealing with strong critical fluctuations in the two-dimensional quantum model. Using standard many-particle techniques a suitable self-consistent approximation can be found and treated with moderate effort, even by analytical means. The approach may serve as a starting point for studying strong fluctuations in the t - J -model at small doping levels. This would require to add bosons representing the doped holes (standard ‘slave-boson’ formulation). Also the connection of the present study to the more general problem of pseudo-gap formation from long-range fluctuations might be helpful for the development of theories for cuprate superconductors. Other possible applications include spin systems like the 2D Heisenberg model with frustration (e.g., the J_1 - J_2 -model) or different lattice geometry, since this merely requires a different density of states corresponding to the interaction function $J(\mathbf{q})$.

Acknowledgments

We acknowledge fruitful discussions on several stages of this work with A. Millis, A. Rosch, A. Ruckenstein, O. F. Syljuåsen, and A.-M. S. Tremblay. This work has been partially supported by the Deutsche Forschungsgemeinschaft.

APPENDIX A: SELF-CONSISTENCY EQUATIONS

1. Equations for Numerical Solution

For a solution of the Eqs.(35) by numerical iteration, retarded propagators are introduced by analytic continuation to the real axis,

$$A(i\nu) \rightarrow A(\omega + i0_+) \equiv A(\omega) = A'(\omega) + iA''(\omega)$$

where $A = \chi, \Pi, D, \Sigma$. In order to avoid the numerical treatment of Bose functions $g(\omega)$ we introduce the structure factors

$$\begin{aligned} S(\mathbf{q}, \omega) &= [1 + g(\omega)] \chi''(\mathbf{q}, \omega) \\ S^0(\omega) &= [1 + g(\omega)] \Pi''(\omega) \\ U(\omega) &= [1 + g(\omega)] D''(\omega) \end{aligned}$$

As will be shown further below, the Eqs.(35) can now be written as

$$S(\mathbf{q}, \omega) = \frac{S^0(\omega)}{|1 + J(\mathbf{q})\Pi(\omega)|^2} \quad (\text{A1a})$$

$$\Pi''(\omega) = S^0(\omega) - S^0(-\omega) \quad (\text{A1b})$$

$$\Pi'(\omega) = \frac{1}{\pi} P \int_{-\infty}^{\infty} d\varepsilon \frac{\Pi''(\varepsilon)}{\varepsilon - \omega} \quad (\text{A1c})$$

$$S^0(\omega) = \frac{\pi}{2} \int_{-\infty}^{\infty} d\varepsilon \rho^+(\varepsilon) \rho^-(\varepsilon - \omega) \quad (\text{A1d})$$

$$\rho^{\{+}\}(\omega) = \begin{cases} 1 - f(\omega) \\ f(\omega) \end{cases} \frac{1}{\pi} \frac{-\Sigma''(\omega)}{|\omega - \Sigma(\omega)|^2} \quad (\text{A1e})$$

$$\begin{aligned} -\Sigma''(\omega) &= \frac{3}{4} \int_{-\infty}^{\infty} d\varepsilon [U(\varepsilon) \rho^-(\varepsilon + \omega) + \\ &\quad + U(-\varepsilon) \rho^+(\varepsilon + \omega)] \end{aligned} \quad (\text{A1f})$$

$$\Sigma'(\omega) = \frac{1}{\pi} P \int_{-\infty}^{\infty} d\varepsilon \frac{-\Sigma''(\varepsilon)}{\omega - \varepsilon} \quad (\text{A1g})$$

$$U(\omega) = S^0(\omega) \int_{-4J}^{4J} d\varepsilon \frac{\mathcal{N}(\varepsilon) \varepsilon^2}{|1 + \varepsilon \Pi(\omega)|^2} \quad (\text{A1h})$$

with the density of states for the nearest-neighbor interaction $J(\mathbf{q})$ in two dimensions,

$$\mathcal{N}(\varepsilon) = \iint_{-\pi}^{\pi} \frac{d^2q}{(2\pi)^2} \delta(\varepsilon - 2J[\cos(q_x) + \cos(q_y)])$$

The temperature enters through the Fermi function $f(\omega)$ in ρ^+, ρ^- . The output from the numerical iteration of these equations is the dynamical spin-structure factor $S(\mathbf{q}, \omega)$, Eq.(A1a), and the spectrum of the auxiliary fermions $\rho(\omega) = [\rho(\omega)^+ + \rho(\omega)^-]$, Eq.(A1e). Furthermore, the static structure factor (equal-time correlation function) is obtained using

$$S^{st}(\mathbf{q}) = \langle S_{\mathbf{q}}^x S_{-\mathbf{q}}^x \rangle = \frac{1}{\pi} \int_{-\infty}^{\infty} d\omega S(\mathbf{q}, \omega) \quad (\text{A1i})$$

In order to save computation time, the wave-vector integral in Eq.(A1h) is done analytically: \mathcal{N} is approximated by its value at the band edges, $\mathcal{N}(\varepsilon) \simeq \frac{1}{4\pi J} \Theta(4J - |\varepsilon|)$. That is, the log-singularity at $\varepsilon = 0$ is ignored, which is anyway suppressed by the factor ε^2 in U . The integral is now easily done, with the result (not writing the ω -arguments)

$$\begin{aligned} U &= \frac{S^0}{\pi 4J |\Pi|^2} \left[8J - \frac{\Pi'}{|\Pi|^2} \ln \left| \frac{(M^+)^2 + (\Pi'')^2}{(M^-)^2 + (\Pi'')^2} \right| + \right. \\ &\quad \left. + \left(1 - \frac{2(\Pi'')^2}{|\Pi|^2} \right) K \right] \quad (\text{A1j}) \end{aligned}$$

$$K = [\arctan(M^+/\Pi'') - \arctan(M^-/\Pi'')]/\Pi''$$

$$M^{\pm} = \Pi' \pm 4J |\Pi|^2$$

At $|\omega| \rightarrow 0$, where $\Pi''(\omega) \propto \omega \rightarrow 0$, we use $K(\omega) = [1/M^-(\omega) - 1/M^+(\omega)]$.

The derivation of Eqs.(A1) goes as follows. Using the spectral representation of the fermion propagator $G(i\omega)$ in Matsubara space,

$$G(i\omega) = \int_{-\infty}^{\infty} d\varepsilon \frac{\rho(\varepsilon)}{i\omega - \varepsilon}$$

the fermion bubble (35a) becomes

$$\Pi(i\nu) = \frac{1}{2} \int_{-\infty}^{\infty} d\varepsilon d\varepsilon' \rho(\varepsilon) \rho(\varepsilon') \frac{f(\varepsilon) - f(\varepsilon')}{i\nu - \varepsilon + \varepsilon'}$$

At the real axis, $i\nu \rightarrow \omega + i0_+$ its imaginary part is multiplied by $[1 + g(\omega)]$ to form the ‘bare’ structure factor,

$$S^0(\omega) = -\frac{\pi}{2} \int_{-\infty}^{\infty} d\varepsilon \rho(\varepsilon) \rho(\varepsilon - \omega) [f(\varepsilon) - f(\varepsilon - \omega)] [1 + g(\omega)]$$

Using $[f(\varepsilon) - f(\varepsilon - \omega)][1 + g(\omega)] = -[1 - f(\varepsilon)]f(\varepsilon - \omega)$, Eq.(A1d) immediately follows. Eq.(A1b) is just a result of the definition of $S^0(\omega)$ and time-reversal symmetry, $\chi''(-\mathbf{q}, -\omega) = -\chi''(\mathbf{q}, \omega)$, $\Pi''(-\omega) = -\Pi''(\omega)$. Similarly the imaginary part of the self energy (35d) reads

$$-\Sigma''(\omega) = \frac{3}{4} \int_{-\infty}^{\infty} d\varepsilon D''(\varepsilon) \rho(\varepsilon + \omega) [g(\varepsilon) + f(\varepsilon + \omega)]$$

With $g + f = g(1 - f) + f(1 + g)$ and $D''(\varepsilon)g(\varepsilon) = D''(-\varepsilon)[1 + g(-\varepsilon)]$, which follows from $D''(-\varepsilon) = -D''(\varepsilon)$, Eq.(A1f) is obtained. The real parts Π' and Σ' are just Kramers–Kronig transformations.

2. Equations for Numerical Solution: Minimal Approximation (MSCA)

The set of equations representing the minimal self-consistent approximation (60) is identical to Eqs.(A1), except that the convolutions in S^0 and Σ'' are missing, i.e., Eqs.(A1d) and (A1f) are to be replaced by

$$S^0(\omega) = \frac{\pi}{4} \rho^+(\omega) \quad (\text{A2})$$

$$-\Sigma''(\omega) = \frac{3}{8} [U(\omega) + U(-\omega)]$$

APPENDIX B: LOCAL SPIN MOMENT

The spin moment $\langle (\mathbf{S}_i)^2 \rangle = 3\langle S_i^x S_i^x \rangle \equiv 3S_{loc}^{st}$ is measured through the local static structure factor

$$\begin{aligned} S_{loc}^{st} &= \frac{1}{N_L} \sum_{\mathbf{q}} S^{st}(\mathbf{q}) \\ &= \int_{-\infty}^{\infty} \frac{d\omega}{\pi} \frac{1}{N_L} \sum_{\mathbf{q}} S(\mathbf{q}, \omega) \\ &= \int_{-\infty}^{\infty} \frac{d\omega}{\pi} S^0(\omega) \int_{-4J}^{4J} d\varepsilon \frac{\mathcal{N}(\varepsilon)}{|1 + \varepsilon \Pi(\omega)|^2} \quad (\text{B1}) \end{aligned}$$

using Eq.(A1a) and the density of states for 2D, introduced in App. A 1. The latter can be written

$$\mathcal{N}(\varepsilon) = \frac{1}{2\pi^2 J} K(m) \Theta(4J - |\varepsilon|) , \quad m = 1 - (\varepsilon/4J)^2$$

with the complete elliptic integral $K(m) = \int_0^1 dt [(1 - t^2)(1 - mt^2)]^{-1/2}$. In contrast to the calculation of $U(\omega)$ in App. A 1 above, it is not suitable to approximate $\mathcal{N}(\varepsilon)$ by a constant, and S_{loc}^{st} is computed numerically from Eq.(B1).

APPENDIX C: DERIVATION OF EQS.(65) FOR THE MSCA

The equations (65) for the analytical treatment of the minimal approximation in Sect. V C is derived from Eqs.(60) as follows: For wave vectors $k \ll 1$, $\mathbf{k} = \mathbf{q} - \mathbf{Q}$, we have $J(\mathbf{q}) \simeq -2dJ + Jk^2$, and the susceptibility (60b) can be written

$$\chi = \frac{1}{J} \left[\left(\frac{1}{J\Pi(0)} - 2d \right) + k^2 + \left(\frac{1}{J\Pi(\omega)} - \frac{1}{J\Pi(0)} \right) \right]^{-1}$$

Introducing the correlation length ξ as in Eq.(39), representing the static and $\tilde{\Pi}(\omega)$ containing the dynamical behavior of χ ,

$$\xi^{-2} = \left(\frac{1}{J\Pi(0)} - 2d \right) , \quad \tilde{\Pi}(\omega) = \Pi(\omega) - \Pi(0)$$

it follows Eq.(65a), with

$$R(\omega) = -\frac{\xi^2}{J} \left(\frac{1}{\Pi(\omega)} - \frac{1}{\Pi(0)} \right) = 2d\xi^2 \frac{2dJ\tilde{\Pi}(\omega)}{1 + 2dJ\tilde{\Pi}(\omega)}$$

Here $\Pi(0) = 1/2dJ$ has been inserted, omitting terms of $\mathcal{O}(\xi^{-2})$. For dispersing peaks (i.e., propagating modes) to be able to appear in $\text{Im}\chi$ for $\xi k > 1$ we may assume that $|R(\omega)| \sim \xi^2 k^2$ and therefore $|\tilde{\Pi}(\omega)| \sim k^2 \ll 1$. In $d = 2$ this leads to Eq.(65b).

The fermion propagator (60e) reads

$$G(i\omega) = \int_{-\infty}^{\infty} d\varepsilon \frac{\rho(\varepsilon)}{i\omega - \varepsilon} \quad (\text{C1})$$

its spectral function $\rho(\varepsilon)$ has been defined in Eq.(65d). Now the irreducible bubble (60a) turns into

$$\Pi(i\nu) = \frac{1}{4} \int_{-\infty}^{\infty} d\varepsilon \rho(\varepsilon) \frac{\tanh(\varepsilon/2T)}{\varepsilon - i\nu}$$

At $i\nu \rightarrow \omega + i0_+$, the imaginary part becomes $\text{Im}\Pi(\omega) = \text{Im}\tilde{\Pi}(\omega) = \frac{\pi}{4} \tanh(\omega/2T) \rho(\omega)$, which forms the imaginary part of Eq.(65c). The expression for $\Pi(0)$ given in Eq.(65g) follows immediately with $\nu = 0$, if the particle-hole symmetry $\rho(\varepsilon) = \rho(-\varepsilon)$ is exploited. The real part of Eq.(65c) comes from $\text{Re}\tilde{\Pi}(\omega) = \text{Re}\Pi(\omega) - \Pi(0)$,

$$\text{Re}\tilde{\Pi}(\omega) = \frac{1}{4} \int_{-\infty}^{\infty} d\varepsilon \tanh(\varepsilon/2T) \rho(\varepsilon) \left[\frac{1}{\varepsilon - \omega} - \frac{1}{\varepsilon} \right]$$

using again $\rho(\varepsilon) = \rho(-\varepsilon)$.

The renormalized interaction (i.e., the local susceptibility) is also written in spectral representation,

$$D(i\nu) = \frac{1}{\pi} \int_{-\infty}^{\infty} d\varepsilon \frac{\text{Im}D(\varepsilon)}{\varepsilon - i\nu} \quad (\text{C2})$$

Inserting this into the self energy (60d) and performing the Matsubara sum results in Eq.(65e).

Finally, D as defined in Eq.(60c) can be written

$$D(\omega) = \iint \frac{d^2q}{4\pi^2} J(\mathbf{q})^2 \frac{\xi^2}{J} \frac{1}{1 + \xi^2 |\mathbf{q} - \mathbf{Q}|^2 - R(\omega)}$$

Here only the contribution from wave vectors \mathbf{q} close to the Néel vector $\mathbf{Q} = (\pi, \pi)$ is reproduced accurately. It is then consistent to let $J(\mathbf{q})^2 \simeq J(\mathbf{Q})^2 = (2dJ)^2$, which leads to Eq.(65f) if $d = 2$.

APPENDIX D: DERIVATION OF THE MSCA FROM THE EQUATIONS OF MOTION

We follow the line of Ref. 67 and consider the general Hamiltonian $H = H_0 + H_1$ for interacting fermions,

$$H_0 = \sum_r \varepsilon_r c_r^\dagger c_r , \quad H_1 = \frac{1}{2} \sum_{r,r',s,s'} V_{s's}^{r'r} c_{r'}^\dagger c_{s'}^\dagger c_s c_r \quad (\text{D1})$$

r collects all single-particle quantum numbers; for the Heisenberg model Eq.(1) it is $r \equiv (i, \alpha)$, and the interaction matrix element reads $V_{j\beta'j\beta}^{ia'\alpha} = J_{ij} \frac{1}{4} \boldsymbol{\sigma}^{\alpha'\alpha} \boldsymbol{\sigma}^{\beta'\beta}$. The commutator of a fermion operator with the Hamiltonian is given by

$$[c_r, H_0] = \varepsilon_r c_r , \quad [c_r, H_1] = \sum_{r_1, r_2, r'_2} V_{r'_2 r_2}^{r r_1} c_{r'_2}^\dagger c_{r_2} c_{r_1} \quad (\text{D2})$$

The propagator for n fermions is defined as

$$G_n(12 \dots n; 1'2' \dots n') = (-1)^n \langle \mathcal{T}_\tau c_1 c_2 \dots c_n c_{n'}^\dagger \dots c_{1'}^\dagger \rangle$$

with the short-hand notation $c_1 \equiv c_{r_1}(\tau_1), c_{1'}^\dagger \equiv c_{r_1'}^\dagger(\tau_1')$ etc. The equations of motion for the 1- and 2-particle Green's function are given by (see, e.g., Ref. 71),

$$(\partial_{\tau_1} + \varepsilon_{r_1}) G(1; 1') = \langle \mathcal{T}_\tau [c_{r_1}, H_1](\tau_1) c_{1'}^\dagger \rangle - \delta(1, 1')$$

$$(\partial_{\tau_1} + \varepsilon_{r_1}) G_2(12; 1'2') = -\langle \mathcal{T}_\tau [c_{r_1}, H_1](\tau_1) c_2 c_{2'}^\dagger c_{1'}^\dagger \rangle - \delta(1, 1') G(2; 2') + \delta(1, 2') G(2; 1')$$

with $\delta(1, 1') \equiv \delta(\tau_1 - \tau_1') \delta_{r_1, r_1'}$. Inserting the commutator (D2) and applying $\int d\mathbf{l} \tilde{G}(3; 1)$ to both sides of the resulting equations, we obtain after re-labeling $1 \rightarrow \bar{1}$, $3 \rightarrow 1$,

$$G(1; 1') = \tilde{G}(1; 1') + \int d\bar{1}' d\bar{1} d\bar{2}' d\bar{2} \tilde{G}(1; \bar{1}') V(\bar{1}' \bar{1}; \bar{2}' \bar{2}) G_2(\bar{1}_- \bar{2}; 1' \bar{2}'_+) \quad (\text{D3})$$

Here $l_\pm \equiv (r_l, \tau_l \pm 0_+)$, $\int d\mathbf{l} \equiv \int_0^\beta d\tau_l \sum_{r_l}$, $V(1'1; 2'2) \equiv V_{r_1' r_1}^{r_2' r_2} \delta(\tau_1' - \tau_1) \delta(\tau_2' - \tau_2) \delta(\tau_1 - \tau_2)$, and \tilde{G} denotes the bare ($V = 0$) Green's function, which fulfills

$$(\partial_{\tau_1} + \varepsilon_{r_1}) \tilde{G}(1; 1') = -\delta(1, 1')$$

Similarly,

$$G_2(12; 1'2') = \tilde{G}(1; 1') G(2; 2') - \tilde{G}(1; 2') G(2; 1') + \int d\bar{1}' d\bar{1} d\bar{2}' d\bar{2} \tilde{G}(1; \bar{1}') V(\bar{1}' \bar{1}; \bar{2}' \bar{2}) G_3(\bar{1}_- \bar{2}; 1' \bar{2}'_+) \quad (\text{D4})$$

The Equations (D3) and (D4) are exact. Self-consistent approximations for the 1-particle Green's function G result from a decomposition of the 3-particle function G_3 in the r.h.s. of Eq.(D4) into lower order propagators. For that we note the generating functional for the n -particle Green's function⁵⁰,

$$Z = \int \mathcal{D}[c, \bar{c}] e^{-A}$$

$$A = \int d\mathbf{l} \bar{c}_1 (\partial_{\tau_1}) c_1 + \int_0^\beta d\tau H(\tau) + \int d\mathbf{l} (\bar{c}_1 \eta_1 + \bar{\eta}_1 c_1)$$

$$G_n(1 \dots n; 1' \dots n') = \frac{1}{Z} \frac{\delta^{2n} Z}{\delta \bar{\eta}_1 \delta \eta_1 \dots \delta \bar{\eta}_n \delta \eta_{n'}} \Big|_{\eta=0}$$

The corresponding connected Green's function is defined as⁵⁰

$$G_n^C(1 \dots n; 1' \dots n') = \frac{\delta^{2n} \ln(Z)}{\delta \bar{\eta}_1 \delta \eta_1 \dots \delta \bar{\eta}_n \delta \eta_{n'}} \Big|_{\eta=0} \quad (\text{D5})$$

Applying Eq.(D5) for $n = 1, 2$ leads to the familiar results $G^C(1; 1') = G(1; 1')$ and

$$G_2^C(12; 1'2') = G_2(12; 1'2') - \{G(1; 1') G(2; 2') - G(1; 2') G(2; 1')\}$$

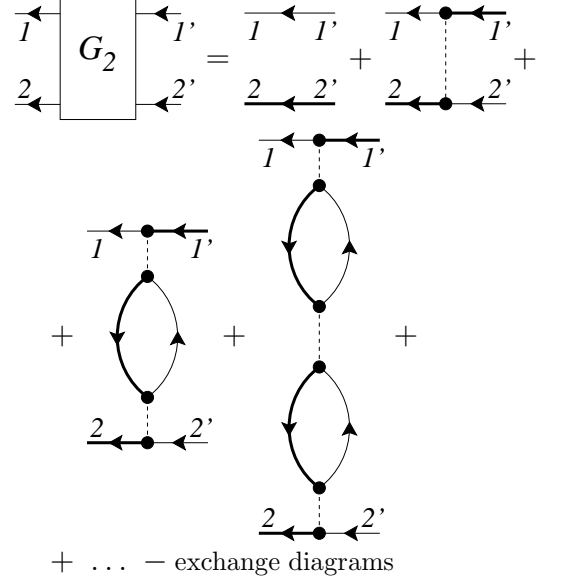


FIG. 12: Diagrammatic representation of Eq.(D7), which has been iterated. All diagrams corresponding to vertex corrections have been omitted, see text. Thin and thick continuous lines denote Green's functions \tilde{G} and G , respectively. The dashed line is $-V$, fermion loops contain a $-$ sign. The exchange diagrams, obtained via $1' \leftrightarrow 2'$, are not shown.

whereas the expression for $n = 3$ reads

$$\begin{aligned} G_3^C(123; 1'2'3') &= G_3(123; 1'2'3') - \\ &- \{ \underbrace{G(1; 1') G_2(23; 2'3')}_{(\text{rpa})} - \underbrace{G(1; 2') G_2(23; 1'3')}_{(\text{rpaex})} + \\ &+ G(1; 3') G_2(23; 1'2') + \text{all other contractions} \} + \\ &+ 2 \{ G(1; 1') G(2; 2') G(3; 3') - \\ &- G(1; 1') G(2; 3') G(3; 2') + \text{all other contractions} \} \end{aligned} \quad (\text{D6})$$

The l.h.s. of Eq.(D6) represents effective 3-particle interactions and is ignored^{36,67}. From the r.h.s. we keep only G_3 and the terms (rpa) and (rpaex), and Eq.(D4) turns into a Bethe-Salpeter equation,

$$\begin{aligned} G_2(12; 1'2') &= \tilde{G}(1; 1') G(2; 2') - \tilde{G}(1; 2') G(2; 1') + \\ &+ \int d\bar{1}' d\bar{1} d\bar{2}' d\bar{2} \tilde{G}(1; \bar{1}') V(\bar{1}' \bar{1}; \bar{2}' \bar{2}) \times \\ &\times \{ G(\bar{1}_-; 1') G_2(2\bar{2}; 2'\bar{2}'_+) - G(\bar{1}_-; 2') G_2(2\bar{2}; 1'\bar{2}'_+) \} \end{aligned} \quad (\text{D7})$$

This equation can now be iterated, leading to an expansion of G_2 in powers of V through the series of particle-hole bubble diagrams shown in Fig. 12.

Note that the bubbles contain one bare \tilde{G} (thin line) and one full Green's function G (full line), which is a direct consequence of the combination $\tilde{G}G$ appearing in the first line of Eq.(D4) and accordingly in (D7). The iteration of Eq.(D7) additionally produces diagrams which

either contribute to vertex corrections to the simple bubbles, or form self-energy insertions of Hartree type. The former have been omitted in Fig. 12. The latter contain loops of the form $\int d\bar{1}'d\bar{1} V(2'2;\bar{1}'\bar{1})g(\bar{1};\bar{1}'_+)\propto\sigma\text{Tr}[\sigma]=0$, $g=\tilde{G}, G$, which are zero for the Heisenberg model without magnetic order. For the same reason the other terms (except (rpa) and (rpaex)) in Eq.(D6) are not considered.

Finally, the G_2 shown in Fig. 12 is inserted in Eq.(D3), omitting again all vertex-correction diagrams that emerge from the contraction of G_2 in (D3). Eq.(D3) now takes the form of a Dyson's equation,

$$G(1;1') = \tilde{G}(1;1') + \int d\bar{1}'d\bar{1} \tilde{G}(1;\bar{1}') \Sigma(\bar{1}';\bar{1}) G(\bar{1};1') \quad (\text{D8})$$

where the self-energy Σ is identified as the series of diagrams obtained from

$$\Sigma(1';1) = \int d\bar{1}'d\bar{1} \hat{V}(1'\bar{1};\bar{1}'1) \tilde{G}(\bar{1};\bar{1}') \quad (\text{D9a})$$

with the renormalized interaction

$$\hat{V}(1'1;2'2) = V(1'1;2'2) + \int d\bar{1}'d\bar{1}d\bar{2}'d\bar{2} V(1'\bar{1};\bar{1}'\bar{1}) G(\bar{1};\bar{2}') \tilde{G}(\bar{2};\bar{1}') \hat{V}(\bar{2}'\bar{2};2'2) \quad (\text{D9b})$$

Eqs.(D8) and (D9) represent exactly the minimal self-consistent approximation given in Fig. 7.

¹ For review and references see Ref. 39.

² B. B. Beard, R. J. Birgeneau, M. Greven, and U.-J. Wiese, Phys. Rev. Lett. **80**, 1742 (1998).

³ J.-K. Kim and M. Troyer, Phys. Rev. Lett. **80**, 2705 (1998).

⁴ M. S. Makivić and H.-Q. Ding, Phys. Rev. B **43**, 3562 (1991).

⁵ N. Elstner, A. Sokol, R. R. P. Singh, M. Greven, and R. J. Birgeneau, Phys. Rev. Lett. **75**, 938 (1995).

⁶ D. P. Arovas and A. Auerbach, Phys. Rev. B **38**, 316 (1988).

⁷ M. Takahashi, Phys. Rev. B **36**, 3791 (1987).

⁸ D. R. Nelson and R. A. Pelkovits, Phys. Rev. B **16**, 2191 (1977).

⁹ See, e.g., Ref. 72 and references therein.

¹⁰ S. Chakravarty, B. I. Halperin, and D. R. Nelson, Phys. Rev. Lett. **60**, 1057 (1988).

¹¹ S. Chakravarty, B. I. Halperin, and D. R. Nelson, Phys. Rev. B **39**, 2344 (1989).

¹² P. Hasenfratz and F. Niedermayer, Z. Phys. B **92**, 91 (1993).

¹³ Y. J. Kim, R. J. Birgeneau, F. C. Chou, M. Greven, M. A. Kastner, Y. S. Lee, B. O. Wells, A. Aharony, O. Entin-Wohlmann, I. Y. Korenblit, et al., Phys. Rev. B **64**, 024435 (2001).

¹⁴ M. Greven, R. J. Birgeneau, Y. Endoh, M. A. Kastner, B. Keimer, M. Matsuda, G. Shirane, and T. R. Thurston, Phys. Rev. Lett. **72**, 1096 (1994).

¹⁵ R. J. Birgeneau, M. Greven, M. A. Kastner, Y. S. Lee, B. O. Wells, Y. Endoh, K. Yamada, and G. Shirane, Phys. Rev. B **59**, 13788 (1999).

¹⁶ B. Keimer, N. Belk, R. J. Birgeneau, A. Cassaho, C. Y. Chen, M. Greven, M. A. Kastner, A. Aharony, Y. Endoh, R. W. Erwin, et al., Phys. Rev. B **46**, 14034 (1992).

¹⁷ Y. Endoh, K. Yamada, R. J. Birgeneau, D. R. Gabbe, H. P. Jennis, M. A. Kastner, C. J. Peters, P. J. Picone, T. R. Thurston, J. M. Tranquada, et al., Phys. Rev. B **37**, 7443 (1988).

¹⁸ M. S. Makivić and M. Jarrell, Phys. Rev. Lett. **68**, 1770 (1992).

¹⁹ G. M. Wysin and A. R. Bishop, Phys. Rev. B **42**, 810 (1990).

²⁰ A. Auerbach and D. P. Arovas, Phys. Rev. Lett. **61**, 617 (1988).

²¹ P. Kopietz, Phys. Rev. Lett. **64**, 2587 (1990).

²² S. Tyč, B. I. Halperin, and S. Chakravarty, Phys. Rev. Lett. **62**, 835 (1989).

²³ D. R. Grempel, Phys. Rev. Lett. **61**, 1041 (1988).

²⁴ Y. J. Kim, R. J. Birgeneau, F. C. Chou, R. W. Erwin, and M. A. Kastner, Phys. Rev. Lett. **86**, 3144 (2001).

²⁵ K. Yamada, K. Kakurai, Y. Endoh, T. R. Thurston, M. A. Kastner, R. J. Birgeneau, G. Shirane, Y. Hidaka, and T. Murakami, Phys. Rev. B **40**, 4557 (1989).

²⁶ S. M. Hayden, G. Aeppli, H. A. Mook, S.-W. Cheong, and Z. Fisk, Phys. Rev. B **42**, 10220 (1990).

²⁷ P. Carretta, A. Rigamonti, and R. Sala, Phys. Rev. B **55**, 3734 (1997), and references therein.

²⁸ A. A. Abrikosov, Physics **2**, 5 (1965).

²⁹ I. Affleck and J. B. Marston, Phys. Rev. B **37**, 3774 (1988).

³⁰ See, e.g., Ref. 73 and references therein.

³¹ M. Inui, S. Doniach, P. J. Hirschfeld, and A. E. Ruckenstein, Phys. Rev. B **37**, 2320 (1988).

³² M. Inaba, H. Matsukawa, M. Saitoh, and H. Fukuyama, Physica C **257**, 299 (1996).

³³ N. E. Bickers, D. J. Scalapino, and S. R. White, Phys. Rev. Lett. **62**, 961 (1989).

³⁴ A. P. Kampf and J. R. Schrieffer, Phys. Rev. B **42**, 7967 (1990).

³⁵ Y. M. Vilk and A.-M. S. Tremblay, J. Phys. I France **7**, 1309 (1997).

³⁶ L. P. Kadanoff and P. C. Martin, Phys. Rev. **124**, 670 (1961).

³⁷ B. R. Patton, Phys. Rev. Lett. **27**, 1273 (1971).

³⁸ B. Jankó, J. Maly, and K. Levin, Phys. Rev. B **56**, R11407 (1997).

³⁹ E. Manousakis, Rev. Mod. Phys. **63**, 1 (1991).

⁴⁰ A. Sokol, R. L. Glenister, and R. R. P. Singh, Phys. Rev. Lett. **72**, 1549 (1994).

⁴¹ A. A. Abrikosov and A. A. Migdal, J. Low Temp. Phys. **3**, 519 (1970).

⁴² P. Coleman, Phys. Rev. B **29**, 3035 (1984).

⁴³ N. E. Bickers, Rev. Mod. Phys. **59**, 846 (1987).

⁴⁴ N. Grewe and H. Keiter, Phys. Rev. B **24**, 4420 (1981).

⁴⁵ Y. Kuramoto, in *Theory of Heavy Fermions and Valence*

Fluctuations, edited by T. Kasuya and T. Saso (Springer, Berlin, 1985), p. 152.

⁴⁶ C. I. Kim, Y. Kuramoto, and T. Kasuya, Sol. State Comm. **62**, 627 (1987).

⁴⁷ W. Metzner and D. Vollhardt, Phys. Rev. Lett. **62**, 324 (1989).

⁴⁸ D. M. Newns and N. Read, Adv. Physics **36**, 799 (1987).

⁴⁹ I. Affleck, Z. Zou, T. Hsu, and P. W. Anderson, Phys. Rev. B **38**, 745 (1988).

⁵⁰ J. W. Negele and H. Orland, *Quantum Many-Particle Systems* (Addison-Wesley, Menlo Park etc., 1988).

⁵¹ L. B. Ioffe and A. I. Larkin, Phys. Rev. B **39**, 8988 (1989).

⁵² J. Kroha, P. J. Hirschfeld, K. A. Muttalib, and P. Wölfle, Sol. State Comm. **83**, 1003 (1992).

⁵³ M. U. Ubbens and P. A. Lee, Phys. Rev. B **46**, 8434 (1992).

⁵⁴ J. Brinckmann and P. A. Lee, Phys. Rev. B **65**, 014502 (2002).

⁵⁵ P. W. Anderson, Science **235**, 1196 (1987).

⁵⁶ J. B. Marston and I. Affleck, Phys. Rev. B **39**, 11538 (1989).

⁵⁷ A. E. Ruckenstein, P. J. Hirschfeld, and J. Appel, Phys. Rev. B **36**, 857 (1987).

⁵⁸ N. Nagaosa and P. A. Lee, Phys. Rev. B **45**, 966 (1992).

⁵⁹ H. Fukuyama, Prog. Theoret. Phys. Suppl. **108**, 287 (1992).

⁶⁰ I. Affleck and F. D. M. Haldane, Phys. Rev. B **36**, 5291 (1987).

⁶¹ A. Singh, Phys. Rev. B **43**, 3617 (1991).

⁶² E. Fradkin, *Field Theories of Condensed Matter Systems* (Addison-Wesley, Reading, MA, 1991).

⁶³ D. Forster, *Hydrodynamic Fluctuations, Broken Symmetry, and Correlation Functions* (Benjamin, Reading, MA, 1975, 1990).

⁶⁴ G. Baym, Phys. Rev. **127**, 1391 (1962).

⁶⁵ J. M. Luttinger and J. C. Ward, Phys. Rev. **118**, 1417 (1960).

⁶⁶ G. Baym and L. P. Kadanoff, Phys. Rev. **124**, 287 (1961).

⁶⁷ P. C. Martin and J. Schwinger, Phys. Rev. **115**, 1342 (1959).

⁶⁸ Q. Chen, I. Kosztin, B. Jankó, and K. Levin, Phys. Rev. B **59**, 7083 (1999).

⁶⁹ Usually the free energy W is constructed as a functional of the full (renormalized) Green's function G and the self energy Σ of the fermions^{64,65}, $W = W[G, \Sigma] = \Phi[G] + \dots$. This leads to Φ -derivable approximations where $\Sigma = \frac{1}{2}\delta\Phi/\delta G$ is a functional of G , while the bare propagator G^0 does not enter Φ , Σ . Alternatively, W can be written as a functional of the renormalized interaction D and its irreducible part Π , $W = W[D, \Pi] = \Phi[D] + \dots$, following the line of Ref. 65. G^0 is considered a constant, like the interaction J , and may enter $\Phi[D]$ and therefore $\Pi = \delta\Phi/\delta D$ to arbitrary order. However, for the particular approximation shown in Fig. 7 we were not able to find the corresponding functional $\Phi[D]$.

⁷⁰ Note that neither a RPA-like bubble series nor vertex corrections to the bubble need to be considered, since the fermion self-energy merely consists of a Hartree diagram with spin–spin interaction.

⁷¹ G. Rickayzen, *Green's Functions and Condensed Matter* (Academic Press, London, 1980).

⁷² D. J. Amit, *Field Theory, the Renormalization Group, and Critical Phenomena* (World Scientific, 1984), 2nd ed.

⁷³ P. W. Anderson, P. A. Lee, M. Randeria, T. M. Rice, N. Trivedi, and F. C. Zhang (2003), preprint cond-mat/0311467.